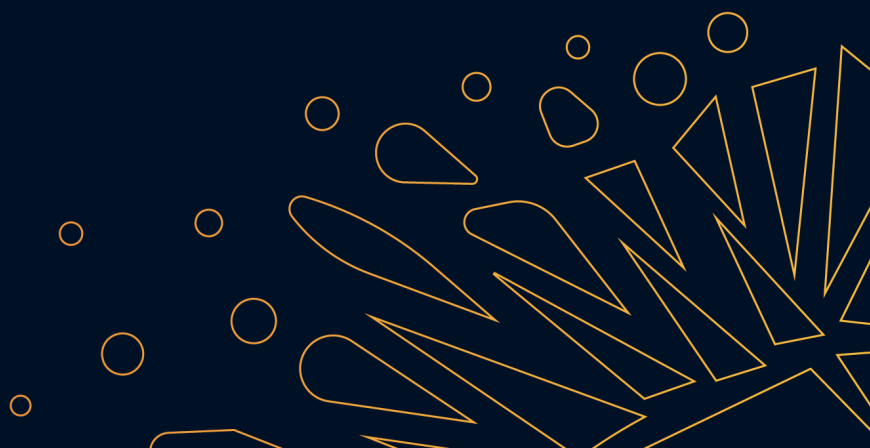


Reducing Electric Furnace Material Physical Property Infrastructure

Theory Manual



Document Purpose

The purpose of this manual is to empower readers to pursue new innovations in the field of pyrometallurgical material property modelling by equipping them with knowledge and understanding of the models available in [auxi-mpp](#).

Target Audience

This user manual is intended for the [Groeien met Groen Staal \(GGS\)](#) consortium involved in developing new [Reducing Electric Furnace \(REF\)](#) technologies, particularly the Theme II partners. It guides users through the underlying theory the material physical property models in [auxi-mpp](#) is based on.

The Theme II partners include process, metallurgical, chemical, and mechanical engineers from Tata Steel Netherlands, along with PhD students and their supervisors from TU Delft, TU Eindhoven, and the University of Twente.

Document Overview

The manual is divided into three parts.

Part I ([Executive Summary](#)) provides an overview of the purpose, contents, and outcomes of this manual. Part II ([Slag Material Properties](#)), covers the theory and validation of the models that describe slag physical properties. And Part III ([Appendices](#)) contains definitions of words and abbreviations used throughout the document.

Disclaimer

This Report has been prepared for the purpose set out in the brief provided to Ex Mente Technologies (Pty) Ltd (Ex Mente) by Groeien met Groen Staal: WP-II.6 (GGS) and was not prepared for any third party or for any other purpose than that detailed in the engagement terms with GGS.

The contents of this document relate specifically to the project referenced herein, and Ex Mente cannot accept responsibility for use of the contents of this document other than for its intended purpose.

The information contained in this document is current as of the date of the Report, and may not reflect any event or circumstance which occurs after the date of the Report.

The opinions contained herein are expressed in good faith and whilst every care has been taken in preparing this Report in accordance with standards of engineering practice (customary in the engineering profession for services of a similar nature), Ex Mente shall not, in any event, be liable for any indirect or consequential damages, including, without limitation, loss of profit or interruption of business arising from the recipient's use of this document or the contents hereof.

Document Identification

Distribution Statement	This document is distributed under the MIT License. Ex Mente retains copyright.
Project Label	NLG-176-603
Project Name	Material Data Framework
Document Name	Reducing Electric Furnace Material Physical Property Infrastructure - Theory Manual
Document Number	NLG-176-603-DOC-1228 Rev. 1
Release Date	2025-07-01
Compiled For	Groeien met Groen Staal: WP-II.6
	Contact person: Vinod Dhiman Tel.: +31 (0)251 49 35 62 E-mail: Vinod.Dhiman@tatasteeleurope.com
Compiled By	Ex Mente Technologies (Pty) Ltd
	Postal address: P.O. Box 10214, Centurion, 0046, SOUTH AFRICA
	Tel.: +27 87 808 1903 E-mail: info@ex-mente.co.za Website: www.ex-mente.co.za

Document Authorisation

Release	Name	Signature
Author	Hanno Muire	
Author	Stefan Koning	
Reviewer	Dr Johan Nell	
Approver	Dr Johan Nell	

Document History

Revision	Release Date	Description
Rev. 1	2025-07-01	Second formal release to GGS.
Rev. 0	2025-02-18	First formal release to GGS.
Draft 1	2025-02-14	Draft 1 release for internal review.

Contents

Title Page	0
Preliminaries	i
Document Purpose	i
Target Audience	i
Document Overview	i
Disclaimer	ii
Document Information	iii
Identification	iii
Authorisation	iv
History	v
Contents	vi
List of Figures	ix
List of Tables	x
I Executive Summary	1
1 Introduction	2
2 Focus	3
3 Highlights	4
II Slag Material Properties	6
4 Density	9
4.1 Thibodeau Density Model	9
4.1.1 Introduction	9
4.1.2 Model Overview	9
4.1.3 Model Formulation	10
Unary	10
Binary	10
Multicomponent	12
Density	12

4.1.4	Variable Declarations	12
4.1.5	Assumptions	13
4.1.6	Model Validation	13
	Molar Volume, Fe-free Systems	13
	Molar Volume, Fe-bearing Systems	20
5	Electrical Conductivity	22
5.1	Thibodeau Electrical Conductivity Model	22
5.1.1	Introduction	22
5.1.2	Model Overview	22
5.1.3	Model Formulation	23
5.1.4	Assumptions	23
5.1.5	Literature Inaccuracies	23
5.1.6	Model Validation	24
5.2	Hundermark Electrical Conductivity Models	30
5.2.1	Introduction	30
5.2.2	Model Overview	30
5.2.3	Model Formulation	30
5.2.4	Assumptions	31
5.2.5	Model Validation	32
6	Diffusivity	37
6.1	Thibodeau Diffusivity Model	37
6.1.1	Introduction	37
6.1.2	Model Overview	37
6.1.3	Model Formulation	38
6.1.4	Variable Declarations	38
6.1.5	Assumptions	38
6.1.6	Simplifications	39
6.1.7	Model Validation	39
7	Viscosity	40
7.1	Grundy-Kim-Brosch Viscosity Model	40
7.1.1	Introduction	40
7.1.2	Model Overview	40
7.1.3	Unary and Binary Model Formulation	41
	Unary Model	41
	Binary Model	41
	Estimating Polymerisation	41
7.1.4	Multicomponent Model Formulation	42
	Systems Without Alumina	42
	Systems Containing Al_2O_3 or Fe_2O_3	43
7.1.5	Variable Declarations	46
7.1.6	Assumptions	47
7.1.7	Simplifications	47
7.1.8	Literature Inaccuracies	47
	Background	47
	Inaccuracies	47
7.1.9	Model Validation	49
	Unary Systems	50

Binary Systems	51
Multicomponent Systems	52
Multicomponent Fe-bearing Systems	55
Issues	57

III Appendices **58**

A Definitions **59**

References **60**

Glossaries **62**

Acronyms 62

List of Figures

4.1	Molar volume vs temperature of unary systems.	15
4.2	Molar volume vs mole fraction of binary systems.	16
4.3	Molar volume vs mole fraction for the ternary systems.	17
4.4	Molar volume vs mole fraction for quaternary systems.	18
4.6	Fraction of non-bridging oxygens for binary systems.	20
5.1	Electrical conductivity vs temperature for unary systems.	25
5.2	Electrical conductivity vs mole fraction of binary systems.	26
5.3	Electrical conductivity vs mole fraction of ternary systems.	27
5.5	Electrical conductivity vs temperature for unary systems.	33
5.6	Electrical conductivity vs mole fraction of binary systems.	34
5.7	Electrical conductivity vs mole fraction of ternary systems.	35
5.8	Electrical conductivity vs mole fraction for FeO – Fe ₂ O ₃ – SiO ₂ system.	36
7.1	Inaccurate plots.	48
7.4	Viscosity model estimates and comparisons for binary slag systems.	52
7.5	Viscosity model estimates for ternary slag systems without alumina.	53
7.6	Viscosity model estimates for ternary slag systems containing alumina.	54
7.7	Viscosity model estimates for the Al ₂ O ₃ – CaO – MgO – SiO ₂ quaternary slag system at 1773 K.	55



List of Tables

4.1	Empirical model parameters for molar volume calculation of SiO_2 slags. . .	12
4.2	Molar Volume Validation Ranges	14
5.1	Electrical Conductivity Validation Ranges	24
5.2	Electrical Conductivity Validation Ranges	32
6.1	Electrical Conductivity Parameters (Thibodeau 2014)	38
7.1	Optimised viscosity parameters	46
7.2	Optimised values of ΔG° for the associate species for slag systems containing $\text{AlO}_{1.5}$ (Grundy et al. 2008a).	46
7.3	Viscosity Validation Ranges	50



Part I

Executive Summary



Chapter 1

Introduction

The pyrometallurgy industry plays an important role in the global economy but faces growing challenges that demand innovative solutions. These challenges include stricter environmental regulations, such as the EU's target of a 30% reduction in CO₂ emissions by 2030, alongside the rising global demand for high-grade steel and increased reliance on lower-quality ores due to the depletion of high-grade resources. Consequently, traditional [Blast Furnace-Basic Oxygen Furnaces \(BF-BOFs\)](#) must be replaced with more efficient smelting technologies, such as the proposed [REF](#) process unit, to help the industry adapt.

Innovation requires advancements in existing tools, particularly in pyrometallurgy. There is a growing need to describe processes more fundamentally through improved material property models, process models, and multiphysics models. These improved models can assist the industry in developing new [REF](#) process units more quickly and cost-effectively.

This manual supports the [GGS](#) Theme II partners in developing new [REF](#) processes with well documented theory on material property models. The property models documented here are implemented in an open-source python package called [auxi-mpp](#). This manual therefore gives the theoretical background and insight necessary to arrive at better innovations using the models available in [auxi-mpp](#).



Chapter 2

Focus

This iteration of the manual covers physical property models for slags, addressing density (molar volume), viscosity, electrical conductivity, and diffusivity. Future versions will expand to include other materials, such as alloys, gases, pellets, and multiphase materials like pellet beds, all accessible through [auxi-mpp](#).

The models take temperature, pressure, composition, and for multi-component models also phase constituent activities, as inputs. The underlying theory for each property model is explained to help readers understand its operation and the specific component systems for which it is valid. The models have been validated against extracted model and experimental data to demonstrate accurate implementation in [auxi-mpp](#).



Chapter 3

Highlights

Density Model (Thibodeau): The Thibodeau density model, which estimates slag density via molar volume, has been successfully implemented in [auxi-mpp](#). This model is fundamentally based on the structural Q-species concept, accounting for variations in melt composition and temperature. The [auxi-mpp](#) implementation demonstrates good agreement with literature models and experimental data for unary, binary, ternary, and quaternary Fe-free systems. For Fe-bearing systems, while parameters have been re-fitted due to changes in Fe bond fraction parameters in the underlying [Modified Quasi-chemical Model \(MQM\)](#) model, further refinement is still required to fully align with extracted literature model data.

Electrical Conductivity Models:

1. **Thibodeau Electrical Conductivity (ThibodeauEC) Model:** This structural model uses the Nernst-Einstein relationship and relies on the molar volume and diffusivity models to predict electrical conductivity. The [auxi-mpp](#) implementation of this model closely reproduces literature and experimental data for unary, binary, and ternary Fe-free systems.
2. **Hundermark Electrical Conductivity Models:** This unified, semi-empirical model is particularly useful for Fe-bearing slags, although it can apply to others. For non-Fe bearing systems, [auxi-mpp](#)'s implementation generally reproduces literature models well, with some exceptions for Al_2O_3 -containing systems. For Fe-bearing systems, current [auxi-mpp](#) estimates deviate from Hundermark's extracted data due to updated Fe bond fraction parameters, necessitating additional validation plots in future updates.

Diffusivity Model (Thibodeau): This model calculates diffusivity from slag polymerisation and is integral to the electrical conductivity calculation within the ThibodeauEC model. While not independently validated due to a lack of direct literature data for comparison, its successful incorporation and indirect validation through the accurate performance of the Thibodeau electrical conductivity model indicate its correctness.

Viscosity Model (Grundy-Kim-Brosch): The Grundy-Kim-Brosch viscosity model has been implemented and successfully validated against literature models and experimental data across unary, binary, and multicomponent systems. For multicomponent Fe-bearing systems, [auxi-mpp](#) generally performs well; however, visible deviations from literature for systems like $\text{CaO} - \text{Fe}_2\text{O}_3 - \text{SiO}_2$ and $\text{Al}_2\text{O}_3 - \text{CaO} - \text{Fe}_2\text{O}_3 - \text{SiO}_2$ were ob-

served, where [auxi-mpp](#)'s results align more closely with [FactSage 8.3](#), suggesting potential inaccuracies in the original literature data or changes in underlying thermodynamic databases.

Part II

Slag Material Properties



Background

Slags are integral to pyrometallurgical processes, serving crucial roles in metal extraction, purification, and environmental control. These molten materials, predominantly composed of metal oxides, form during the smelting, refining, and alloying of metals. Slags not only facilitate the separation of metals from their ores but also play a significant role in controlling reactions, heat transfer, and minimising environmental impacts such as emissions and waste generation. Controlling the slag properties is therefore essential for optimal yields and minimal waste. To effectively control slag properties, it is important to understand the underlying principles that govern them.

The physical properties of slags are intricately interconnected, primarily due to the slag's structure. This structure, specifically the degree of polymerisation (Q) of the silicate network, acts as the fundamental characteristic influencing the slag's properties like diffusivity (D), viscosity (μ), electrical conductivity (σ), thermal conductivity (κ), and density (ρ) (Mysen and Richet 2019).

A highly polymerised network, characterised by long, interconnected chains of silicate tetrahedra, restricts the movement of all slag components. This restricted movement results in higher μ , as the slag becomes more resistant to flow. Similarly, D decreases, as the interconnected network hinders the movement of ions. σ is also reduced, as the movement of charge-carrying cations is impeded by the tightly bound structure. κ is increased, as the interconnected structure presents a lower resistance to the flow of phonons, resulting in higher thermal conductivity.

Conversely, a less polymerised network with more non-bridging oxygen atoms, allows for greater freedom of movement. This leads to lower μ , higher D , increased σ , but decreased κ . The molar volume (\bar{V}) and ρ is also affected by Q , as the arrangement of silicate tetrahedra and the packing of cations influence the overall volume occupied by the slag.

The structure of silicate melts is characterised by the three types of bridging oxygen atoms. A free oxygen separates a metal-metal (M – M) pair, a non-bridging oxygen separates a metal-silicon (M – Si) pair, and a bridging oxygen separates a silicon-silicon (Si – Si) pair. From the Si atom's perspective, silicon atoms are always tetrahedrally bonded to four oxygen ions such that the basic silicate melts mainly consist of M^{q+} , O^{2-} , and SiO_4^{4-} . As the silica content increases beyond the orthosilicate composition, the SiO_4^{4-} tetrahedra begin to polymerise, forming more bridging oxygens and gradually creating a three-dimensional network.

The degree of polymerisation of a slag is described by the Q^n -species which is the fraction of SiO_4^{4-} ions that contains n bridging oxygens. In pure SiO_2 , all four oxygens surrounding each silicon are bridging oxygens, with the Q^4 -species fraction being 1.0,

whereas an isolated SiO_4^{4-} ion is a Q^0 -species (Kim et al. 2012a).

The structure of a slag is significantly affected by both temperature (T) and composition (x). Increasing T generally leads to a decrease in polymerisation, as the thermal energy breaks the bonds between silicate tetrahedra, resulting in shorter chains and a more fluid slag. x also plays a crucial role, with network-forming oxides like SiO_2 and Al_2O_3 promoting polymerisation by forming extensive interconnected networks. Conversely, network-modifying oxides such as CaO , MgO , Na_2O , and K_2O disrupt the network by breaking the $\text{Si}-\text{O}-\text{Si}$ bonds, resulting in shorter chains and a less polymerised structure. Al_2O_3 is also amphoteric and may act as a network modifier depending on the availability of other network-modifying oxides, such as CaO or Na_2O , to charge compensate for Al^{3+} ions.

In short, the specific type and concentration of these oxides, along with T , ultimately determine the structure and resulting physical properties of slag.

Chapter 4

Density

4.1 Thibodeau Density Model

A model developed by Thibodeau et al. ([2016a](#)).

4.1.1 Introduction

The density is closely related to the molar volume of a slag, it is essentially the reciprocal thereof. Estimation of the density is therefore not limited to models strictly for density, as molar volume models will achieve the same goal. Hence, the structural molar volume model developed by Thibodeau et al. ([2016a](#)) was implemented with the intention to estimate slag density.

4.1.2 Model Overview

This model is based on the concept of silicate tetrahedral Q -species. Q -species represent different structural units defined by silicon tetrahedra with varying numbers of bridging oxygens (oxygen atoms shared between two tetrahedra), non-bridging oxygens (oxygen atoms bonded to only one silicon atom), and free oxygens (oxygen atoms not bonded to silicon).

The original literature model uses the [MQM](#) found in [ChemApp for Python](#) and the FactSage FToxid database to calculate the quantity of each Q -species in a given melt (Thibodeau et al. [2016a](#)). Each Q -species is assigned a molar volume that changes linearly with temperature. The model calculates the total molar volume of the melt by summing the contributions from each Q -species and free oxide species. This allows the model to account for the non-linear behaviour of molar volume in silicate melts that arises from the changing distribution of Q -species with composition and temperature.

It is important to note that this model is formulated strictly for liquid slag systems – the user should therefore ensure that his/her system is above the liquidus temperature before performing calculations. Also, we recommend the model to be used within the validation ranges specified in [Table 4.2](#). The validation ranges are based on selected figures from the original articles. To peruse the full range of systems the model were validated for, the user is directed to the original article.

Finally, for systems containing Fe, the correct ratio of Fe(II) and Fe(III) has to be provided. This means the user needs to know the oxidation environment of the system, and from that estimate this ratio before passing it on to the model.

4.1.3 Model Formulation

Molar volume for a multicomponent system is typically expressed with Equation (4.1).

$$\bar{V}_{\text{slag}} = \frac{\sum_i \bar{m}_i \cdot x_i}{\rho_{\text{slag}}} \quad (4.1)$$

However, the molar volume of the metal oxide melt (slag) can also be expressed as the sum of molar volumes for each phase constituent scaled by its mole fraction in the slag, according to Equation (4.2).

$$\bar{V}_{\text{slag}} = \sum_i \bar{V}_i \cdot x_i \quad (4.2)$$

Thibodeau et al. (2016a) and Thibodeau et al. (2016b) developed more fundamental, structure-based equations based on Equations (4.1) and (4.2) to model the molar volume in binary and multicomponent slag systems containing $\text{Li}_2\text{O} - \text{Na}_2\text{O} - \text{K}_2\text{O} - \text{MgO} - \text{CaO} - \text{MnO} - \text{PbO} - \text{Al}_2\text{O}_3 - \text{SiO}_2$. This model was further extended to include FeO and Fe_2O_3 in Thibodeau et al. (2016c), demonstrating its applicability across a wide range of SiO_2 -based slag systems. The following information describes the model and its implementation.

Unary

The molar volume of a unary system is simply calculated as a linear combination of a pure oxide's parameters at a specific temperature, as shown in Equation (4.3).

$$\bar{V}_{\text{slag}}^T = a + bT \quad (4.3)$$

Binary

The level of oxygen in slag determines the types and quantities of bonding scenarios that develop between non-oxygen atoms. There are types of bonding scenarios corresponding to the three possible structural states for oxygen shown in Equation (4.4). O^0 represents a bridging oxygen; $\text{Si} - \text{O} - \text{Si}$, O^{2-} refers to a free oxygen; $\text{M} - \text{O} - \text{M}$, and O^- denotes a non-bridging oxygen; $\text{Si} - \text{O} - \text{M}$.



If we are dealing with one mole of slag, the total moles of oxygen per mole of slag is calculated by summing the oxygen contributions from each species in the slag system, as shown in Equation (4.5).

$$n_t = x_{M_2O} + x_{MO} + 3x_{M_2O_3} + 2x_{MO_2} \quad (4.5)$$

The number of bridging oxygen atoms is calculated using Equation (4.6), which incorporates the bond fraction of Si – O – Si contacts and can be obtained from the MQM model found in [ChemApp for Python](#). Likewise, Equation (4.7) is used to determine the number of M – O – M contacts.

$$n_{O^0} = x_{Si-Si} \cdot n_t \quad (4.6)$$

$$n_{M-M} = x_{M-M} \cdot n_t \quad (4.7)$$

Now, the number of Si – O⁰ bonds per mole of solution is simply twice the number of bridging oxygens; $2n_{O^0}$. The average number of bridged oxygens per silicon atom is therefore $2n_{O^0}/x_{SiO_2}$. Assuming that all Si atoms are tetrahedrally coordinated with four oxygens, the probability that one of the oxygens will be bridging is therefore a quarter of this, as given by Equation (4.8).

$$P_{O^0} = \frac{1}{4} \cdot \frac{2n_{O^0}}{x_{SiO_2}} = \frac{n_{O^0}}{2x_{SiO_2}} \quad (4.8)$$

If the probability of an oxygen in a Q -species being a bridging oxygen is known, the probability to have a given Q^n (where $n = 0, 1, 2, 3$, or 4) can be calculated with Equation (4.9);

$$W_n = \frac{4!}{(4-n)!n!} P_{O^0}^n (1 - P_{O^0})^{(4-n)} \quad n = 0, 1, 2, 3, \text{ or } 4 \quad (4.9)$$

The amount of each Q -species per mole of slag can be determined from their probabilities to form, calculated with Equation (4.10). This is achieved by multiplying W_n with x_{SiO_2} , since the latter gives the mole fraction of all Q -species combined;

$$n_{Q^n} = W_n \cdot x_{SiO_2} \quad \text{for } n = 0, 1, 2, 3, \text{ or } 4 \quad (4.10)$$

The molar volume is then calculated by Equation (4.11) as a linear combination of the molar volume for each species, weighted by the amount of the associated species present.

$$\bar{V}_{slag}^T = n_{Q^4} \bar{V}_{SiO_2}^T + \sum_{n=0}^3 n_{Q^n} \bar{V}_{Q^n}^T + n_{M-M} \bar{V}_{M-M}^T \quad (4.11)$$

In Equation (4.11), the species specific molar volume is calculated with Equation (4.12), where the two empirical parameters a and b were fitted to the pure oxide slags, assuming that their molar volumes varies linearly with temperature.

$$\bar{V}_i = a_i + b_i T \quad (4.12)$$

Multicomponent

To calculate the molar volume for multicomponent systems, Equation (4.11) was adapted to account for the different cations that Si can be connected to and for the different ways in which the cations can connect to each other. This is given in Equation (4.13). The molar volume of a given Q -species is therefore calculated as a linear combination of the different non-bridging oxygen, Si – M_j , scenarios. The contribution from free oxygen contacts, $\bar{V}_{M_i-M_j}^T$, are taken as the average of their pure oxides' molar volumes as per Equation (4.14).

$$\bar{V}_{\text{slag}}^T = n_{Q^4} \bar{V}_{\text{SiO}_2}^T + \sum_{n=0}^3 n_{Q^n} \frac{\sum_i x_{\text{Si}-M_i} \bar{V}_{Q^n}^T}{\sum_i x_{\text{Si}-M_i}} + \sum_i \sum_j n_{M_i-M_j} \bar{V}_{M_i-M_j}^T \quad (4.13)$$

$$\bar{V}_{M_i-M_j}^T = \frac{\bar{V}_{M_i}^T + \bar{V}_{M_j}^T}{2} \quad (4.14)$$

Density

Once the molar volume is known, the density can be calculated. The density can be calculated from molar volume with Equation (4.15).

$$\rho_{\text{slag}} = \frac{\sum_i \bar{m}_i x_i}{\bar{V}_{\text{slag}}} \quad (4.15)$$

If the molar volume model proves to be accurate, accurate density values can be calculated from it.

4.1.4 Variable Declarations

The parameters used in Equation (4.12) is tabulated in Table 4.1

Table 4.1: Empirical model parameters for molar volume calculation of SiO₂ slags.

Oxides	Q^3		Q^2		Q^1		Q^0		Pure Oxide	
	a	b × 10 ³	a	b × 10 ³	a	b × 10 ³	a	b × 10 ³	a	b × 10 ³
SiO ₂	-	-	-	-	-	-	-	-	27.3	0.00
Li ₂ O	29.96	2.80	35.73	5.00	41.66	6.50	48.18	8.20	13.52	3.30
Na ₂ O	34.41	3.50	43.11	8.00	53.22	10.0	63.78	13.0	25.32	5.95
K ₂ O	38.17	6.00	54.75	12.00	68.92	16.50	87.63	21.00	37.85	8.83
MgO	30.42	1.00	34.79	2.40	37.66	4.00	42.34	5.00	14.05	0.70
CaO	32.60	1.70	35.60	3.50	42.60	6.00	50.70	7.00	19.54	0.85
MnO	31.00	1.60	34.50	3.50	38.80	6.50	43.00	7.00	16.09	0.95
PbO	39.00	1.00	44.50	3.00	56.00	5.00	65.00	8.30	23.86	3.21
Al ₂ O ₃	35.98	0.00	36.89	0.00	47.69	0.00	50.30	0.00	11.15	0.47
FeO*	29.90	3.50	31.10	2.00	40.80	5.20	48.70	6.70	13.46	1.17
Fe ₂ O ₃ *	40.60	0.00	48.20	0.00	82.60	0.00	44.20	0.00	10.05	1.38

* The model parameters for FeO and Fe₂O₃ had to be refitted due to a change in Fe parameters used in the MQM model of ChemApp for Python.

4.1.5 Assumptions

The structural molar volume model for oxide slags is based on several key assumptions.

1. It relies on accurately estimated molar volumes of pure liquid oxide components.
2. It assumes that the molar volume of each component, including pure oxides and Q -species, changes linearly with temperature.
3. The model uses Q -species as the fundamental structural units, assuming they are the minimal units needed to explain silicate melt volumes.
4. It considers the excess molar volume from medium-range structures formed by Q -species to be negligible.
5. It assumes that the [MQM](#), with the [FactSage](#) FToxid database, accurately calculates bond fractions.
6. It assumes a single liquid melt without solid phases or liquid miscibility gaps.
7. It assumes Al_2O_3 to be a network modifier.
8. It assumes other potentially important anions (e.g. S^{2-} , SO_4^{2-} , CO_3^{2-} , etc.) will not disrupt the oxygen network.

4.1.6 Model Validation

Molar Volume, Fe-free Systems

The Thibodeau density model implemented in [auxi-mpp](#), was evaluated by comparing its inverse (molar volume) against both the literature model and experimental data. Data were extracted directly from figures in Thibodeau et al. (2016a) and Thibodeau et al. (2016b). The models were validated for the systems and temperatures shown in Table 4.2.

Table 4.2: Molar Volume Validation Ranges

Model	Systems	Composition (mol mol ⁻¹)	Temperature (K)
Unary	SiO ₂	pure substance	0 – 3000
	Al ₂ O ₃	pure substance	2000 – 3250
	MgO	pure substance	300 – 4000
	CaO	pure substance	300 – 3500
Binary	Al ₂ O ₃ – SiO ₂	$x_{\text{Al}_2\text{O}_3} = 0 - 1$	2073
	CaO – SiO ₂	$x_{\text{CaO}} = 0 - 1$	1773, 1973
	MgO – SiO ₂	$x_{\text{MgO}} = 0 - 1$	1973
Ternary	CaO – MgO – SiO ₂	$x_{\text{MgO}} = 0 - 1, x_{\text{SiO}_2}/x_{\text{CaO}} = 1$	1723, 1873
	CaO – MgO – SiO ₂	$x_{\text{CaO}} = 0 - 1, x_{\text{SiO}_2}/x_{\text{MgO}} = 2$	1723, 1873
	Al ₂ O ₃ – MgO – SiO ₂	$x_{\text{SiO}_2} = 0 - 1, x_{\text{MgO}}/x_{\text{Al}_2\text{O}_3} = 1$	1873, 1973
	Al ₂ O ₃ – MgO – SiO ₂	$x_{\text{MgO}} = 0 - 0.5, x_{\text{SiO}_2} = 0.5$	1873, 1973
	Al ₂ O ₃ – CaO – SiO ₂	$x_{\text{SiO}_2} = 0 - 1, x_{\text{CaO}}/x_{\text{Al}_2\text{O}_3} = 1$	1773, 1873
	Al ₂ O ₃ – CaO – SiO ₂	$y_{\text{Al}_2\text{O}_3, \text{CaO}, \text{SiO}_2} = 0 - 1$	1873
	CaO – MgO – SiO ₂	$y_{\text{CaO}, \text{MgO}, \text{SiO}_2} = 0 - 1$	1873
Quaternary	Al ₂ O ₃ – CaO – MgO – SiO ₂	$y_{\text{Al}_2\text{O}_3, \text{CaO}, \text{SiO}_2} = 0 - 0.9, y_{\text{MgO}} = 0.1$	1873
	Al ₂ O ₃ – CaO – MgO – SiO ₂	$y_{\text{CaO}, \text{MgO}, \text{SiO}_2} = 0 - 0.8, y_{\text{Al}_2\text{O}_3} = 0.2$	1873
	Al ₂ O ₃ – CaO – MgO – SiO ₂	$y_{\text{CaO}, \text{MgO}, \text{SiO}_2} = 0 - 0.7, y_{\text{Al}_2\text{O}_3} = 0.3$	1873

The [auxi-mpp](#) model agrees well with the literature model across unary, binary, ternary and quaternary systems. Figure 4.1 shows that [auxi-mpp](#) aligns with the literature model (“2016: Thibodeau et al.”) for unary systems, plotting molar volume against temperature.

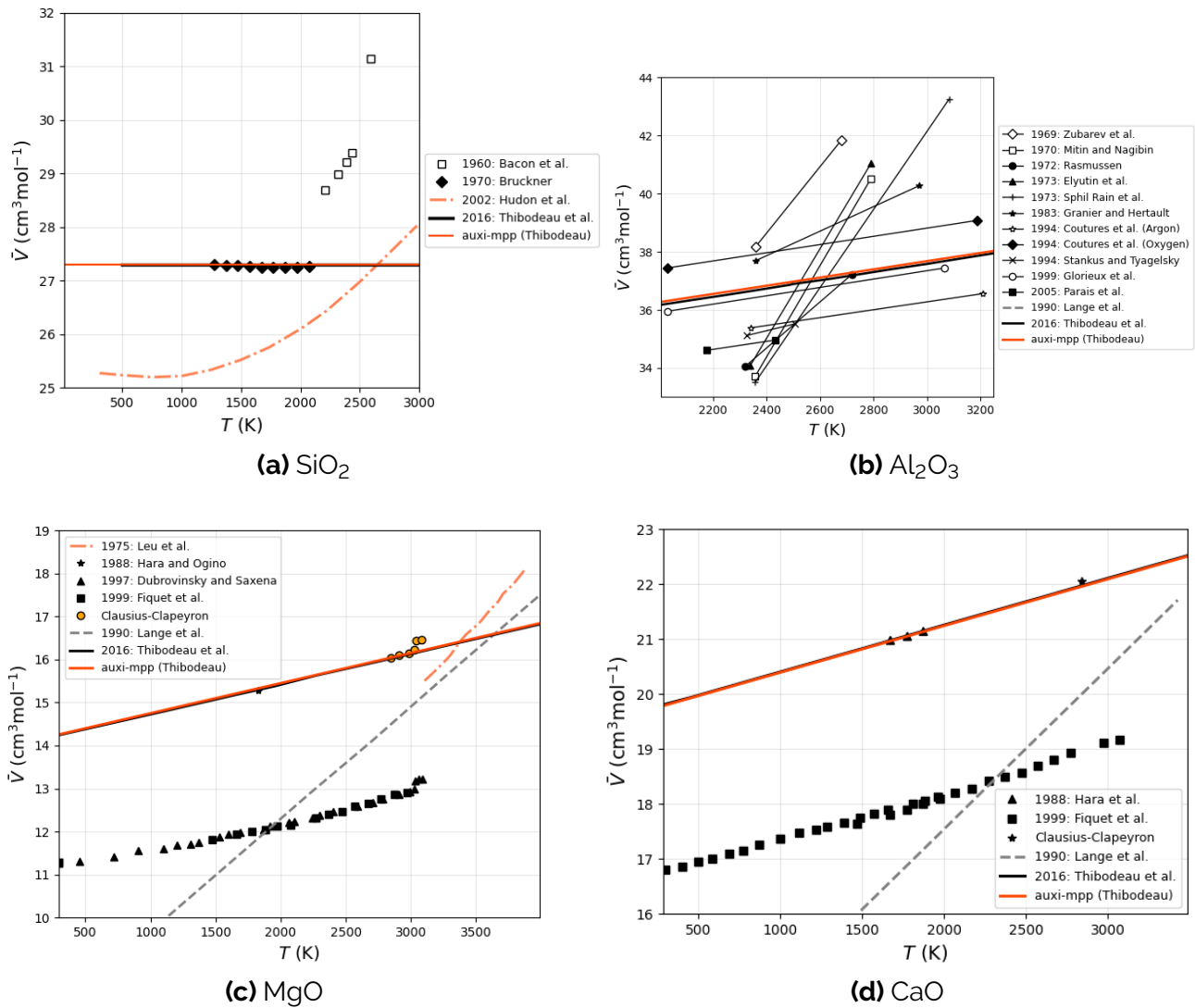


Figure 4.1: Molar volume vs temperature of unary systems.

Similarly, Figure 4.2 and Figure 4.3 confirm this agreement for binary and ternary systems, where molar volume is plotted against mole fraction.

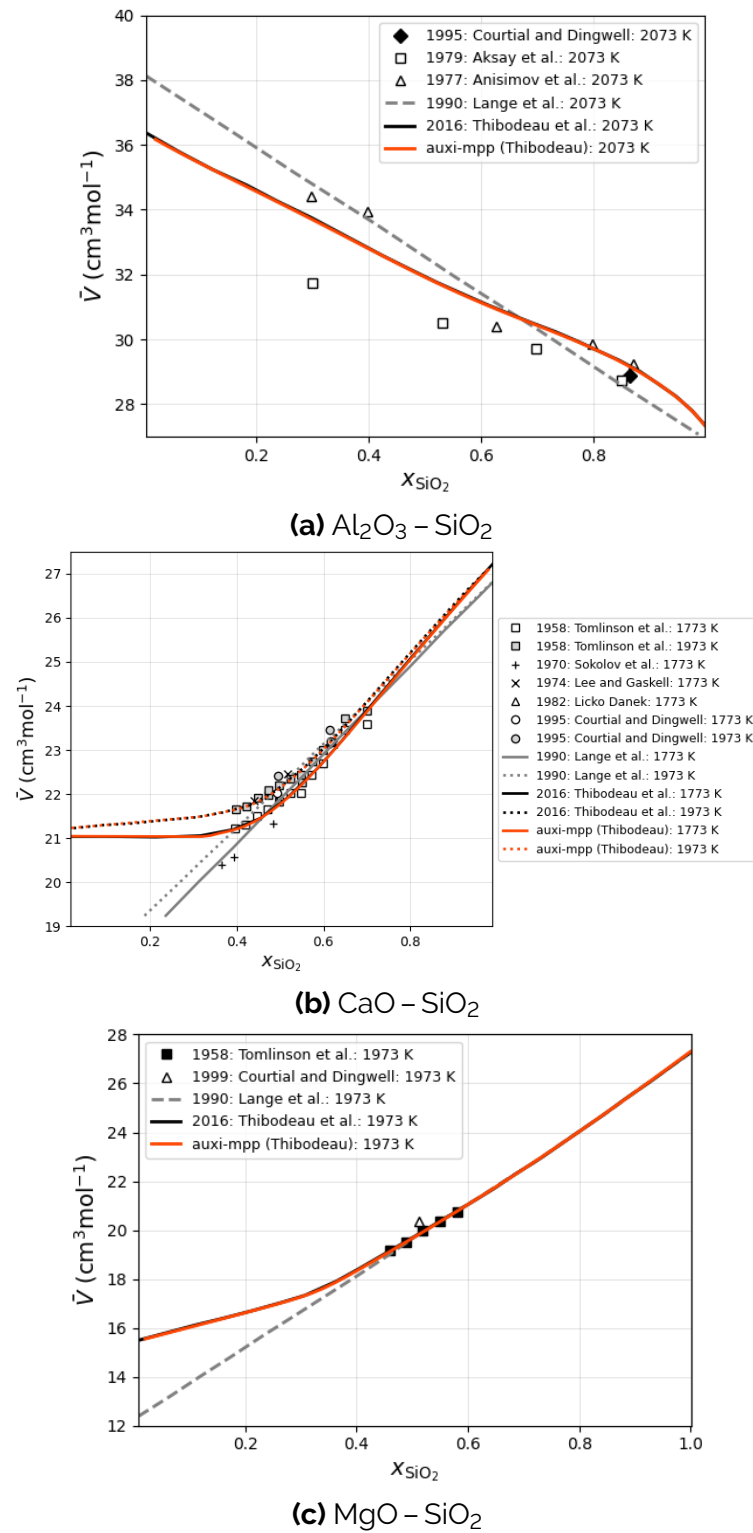


Figure 4.2: Molar volume vs mole fraction of binary systems.

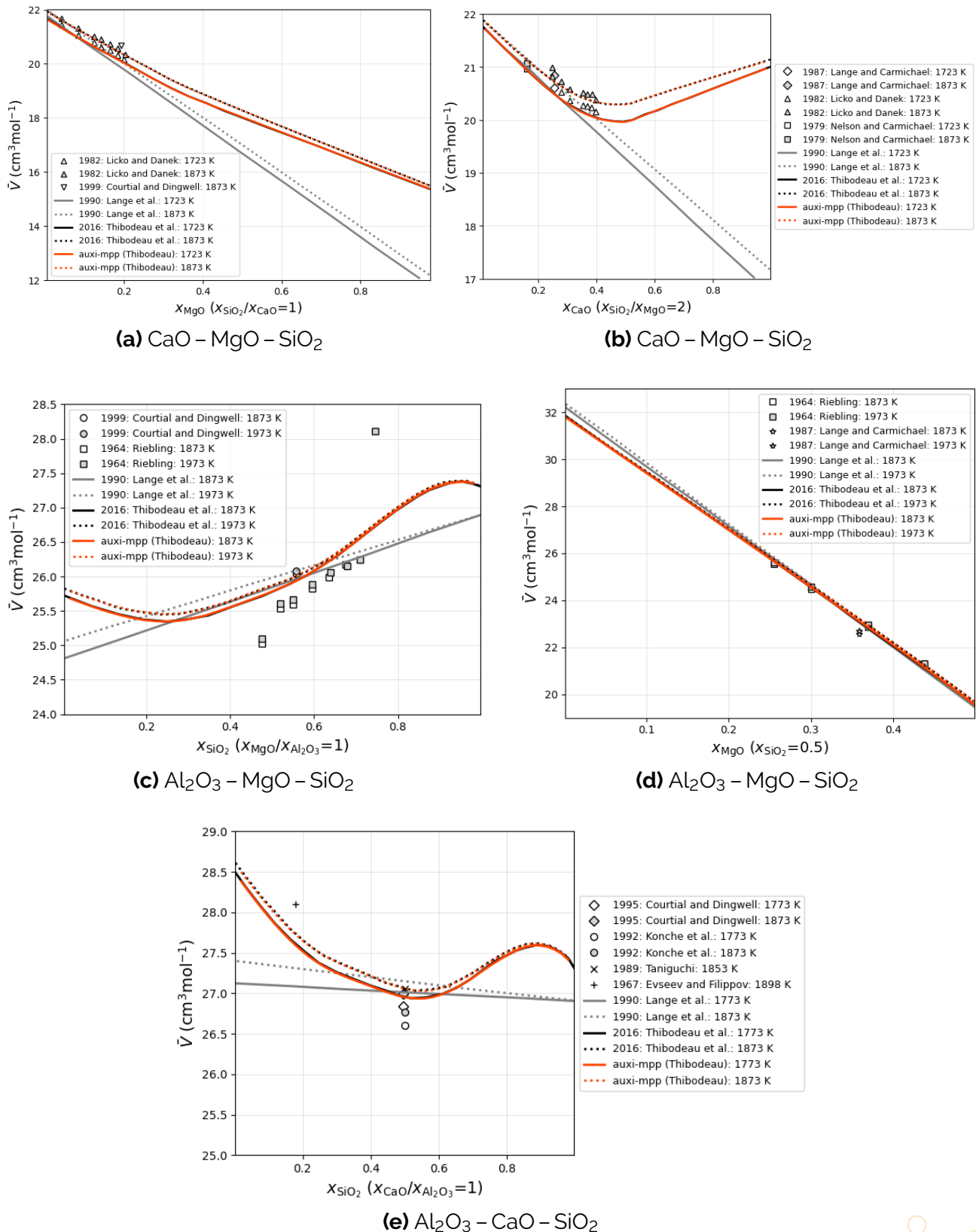
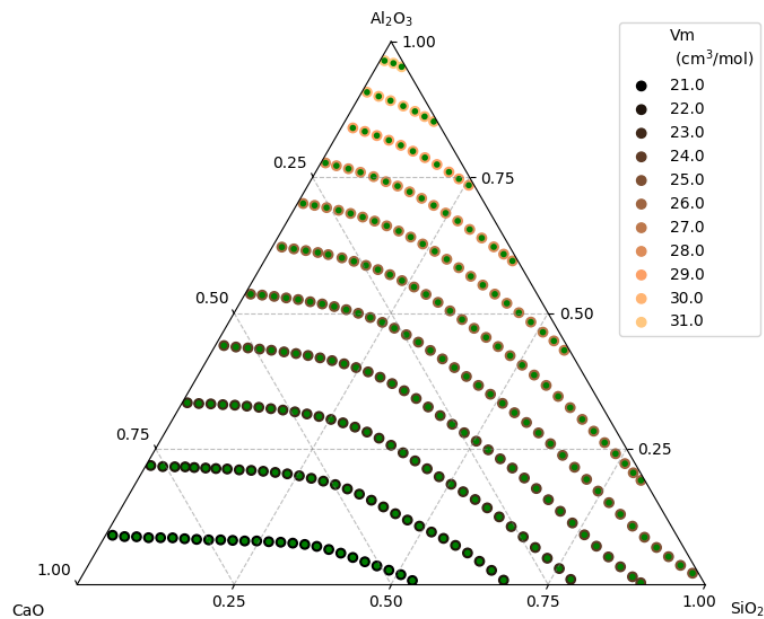


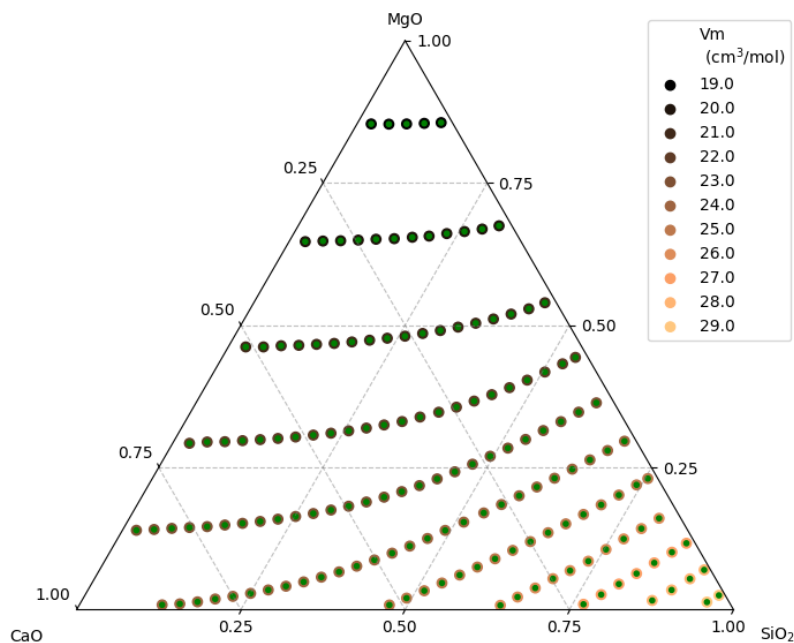
Figure 4.3: Molar volume vs mole fraction for the ternary systems.

auxi-mpp was also validated for Al₂O₃ – CaO – MgO – SiO₂. In Figure 4.4, the ternary diagrams display the molar volume contour lines as calculated by Thibodeau et al. (2016b). For each point on the contour line, the composition were extracted and used to calculate the molar volume using **auxi-mpp** to see if the contour line's value could be reproduced.

The green points in Figure 4.4 indicate [auxi-mpp](#)'s estimations that lies within a 1% error threshold compared to the value of the contour line.



(a) $\text{Al}_2\text{O}_3 - \text{CaO} - \text{MgO} - \text{SiO}_2$ system at 1873 K and $y_{\text{MgO}} = 0.1$



(b) $\text{Al}_2\text{O}_3 - \text{CaO} - \text{MgO} - \text{SiO}_2$ system at 1873 K and $y_{\text{Al}_2\text{O}_3} = 0.3$

Figure 4.4: Molar volume vs mole fraction for quaternary systems.

Finally, Figure 4.5 gives an oversight of how [auxi-mpp](#) compares with literature for ternary and quaternary systems.

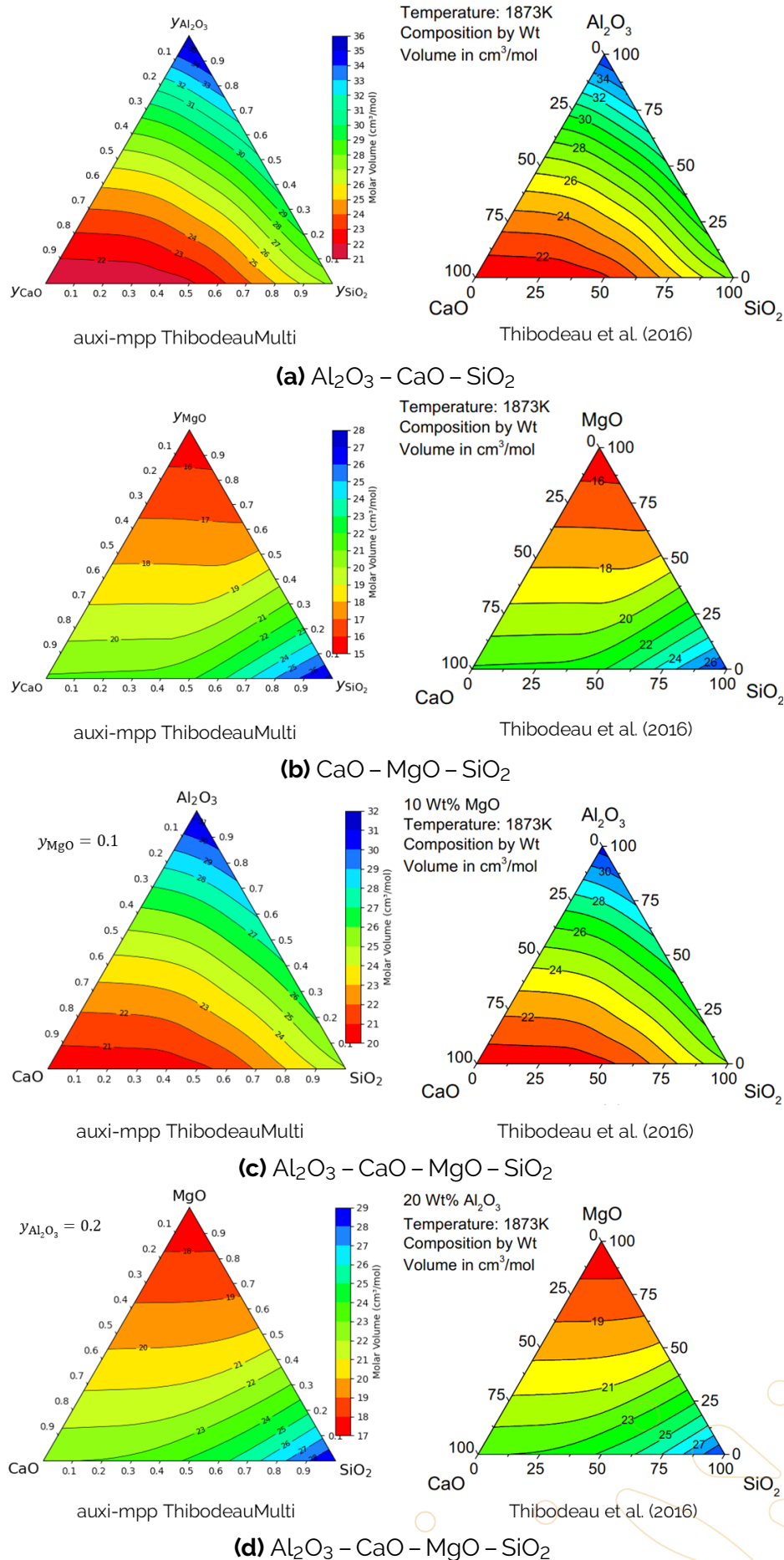


Figure 4.5: Comparing auxi-mpp's contour plots with literature.

Molar Volume, Fe-bearing Systems

The original parameters were refitted due to a change in the Fe parameters used in the MQM model of ChemApp for Python which resulted in a change in bond fraction estimates. This is shown with Figure 4.6 for the fraction of non-bridging oxygens in the SiO_2 – FeO system compared to SiO_2 – CaO and SiO_2 – MgO systems.

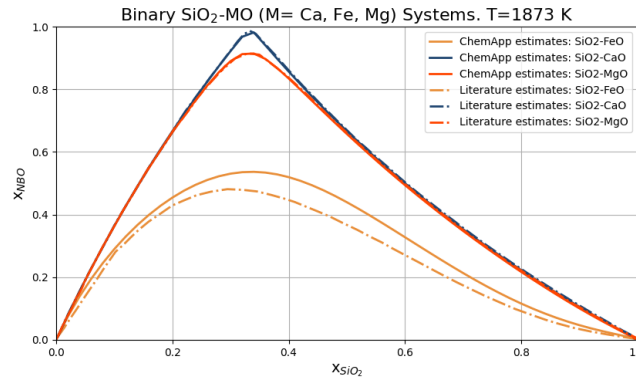
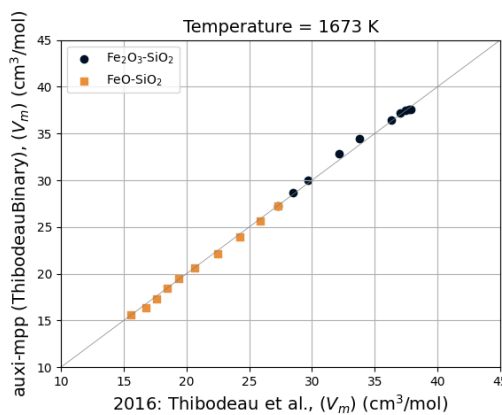


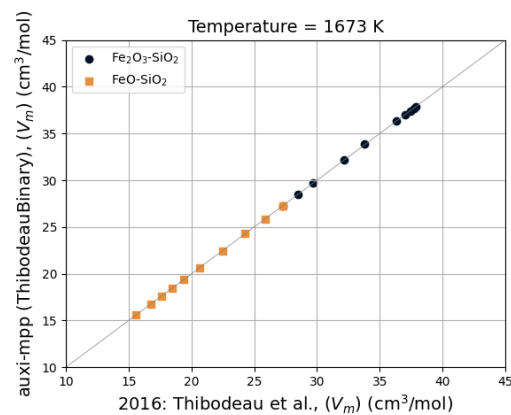
Figure 4.6: Fraction of non-bridging oxygens for binary systems.

Correlation plots were generated for the following Fe-bearing systems using both the original and the updated parameters for FeO and Fe_2O_3 from Table 4.1. There is still deviation between the extracted model data and estimated model data from [auxi-mpp](#) with respect to temperature as shown in Figure 4.8. Further refinement of the parameters are required and will be addressed in a later update.

1. FeO – SiO_2 (Hypothetical)
2. Fe_2O_3 – SiO_2 (Hypothetical)
3. Fe_2O_3 – FeO – SiO_2
4. CaO – Fe_2O_3 – FeO – SiO_2

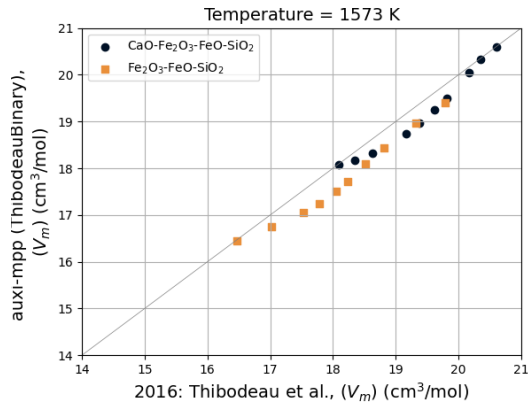


(a)

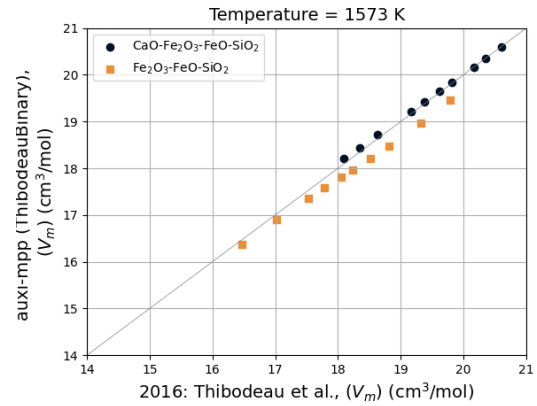


(b)

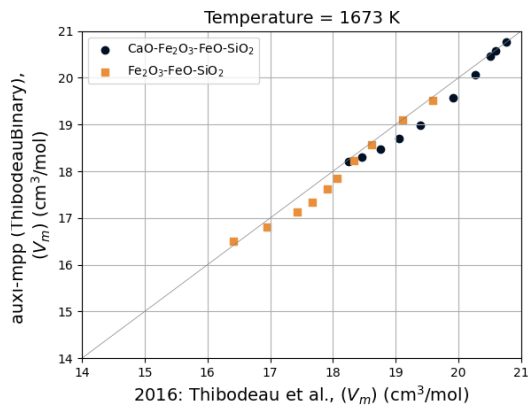
Figure 4.7: [auxi-mpp](#) vs Thibodeau (2014) for correlation plots for hypothetical Fe-bearing binary systems, original (left) and updated (right) for FeO and Fe_2O_3 parameters.



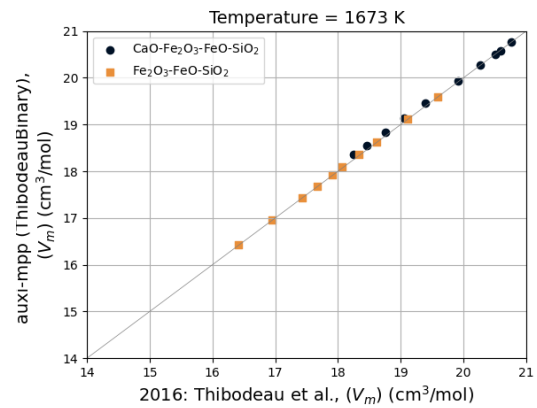
(a)



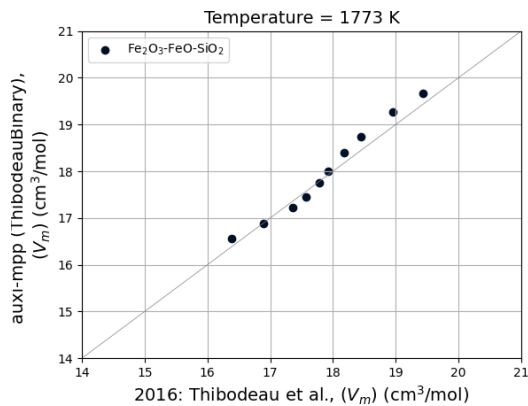
(b)



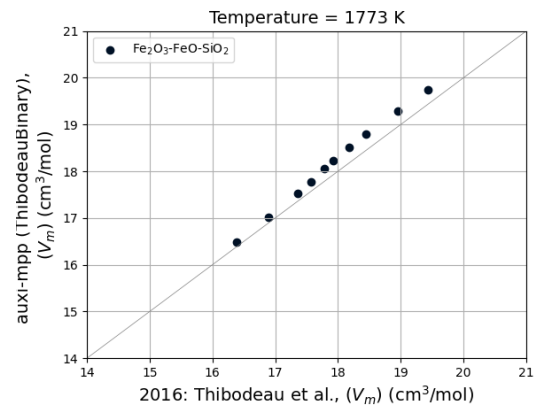
(c)



(d)



(e)



(f)

Figure 4.8: auxi-mpp vs Thibodeau (2014) correlation plots, original (left) and updated (right) for FeO and Fe₂O₃ parameters.

Chapter 5

Electrical Conductivity

5.1 Thibodeau Electrical Conductivity Model

A model developed by Thibodeau (2016).

5.1.1 Introduction

The electrical conductivity model is a structural model that uses the Nernst-Einstein relationship to predict the electrical conductivity of oxide melts. The model is built on the concept of ionic conduction, where cations act as charge carriers, and their movement is influenced by the slag's polymerisation.

5.1.2 Model Overview

The model relies on Thibodeau's molar volume (density) model, Chapter 4, to calculate the degree of polymerisation (Q), enabling it to account for variations in melt composition. Its parameters for individual cations are derived from unary and binary silicate systems, allowing it to estimate the electrical conductivities of higher-order systems without additional parameters.

The model only deals with the role of ionic conduction in the electrical conductivity of oxide melts. When these melts contain substantial amounts of iron oxide and manganese oxide (transition metal oxides), they can host significant quantities of both divalent and trivalent Fe and Mn cations. In such instances, the contribution of electronic conduction to electrical conductivity must also be considered. Thibodeau (2014) does consider Fe^{2+} and Fe^{3+} electronic contributions in a later modified version of his model, but indicates that the model is not reliable for estimating electrical conductivity in Fe-bearing systems. It is recommended to use Hundermark's unified model, Equation (5.4), for systems containing FeO and Fe_2O_3 .

It is important to note that this model is formulated strictly for liquid slag systems – the user should therefore ensure that his/her system is above the liquidus temperature before performing calculations. Also, we recommend the model to be used within the validation ranges specified in Table 5.1. The validation ranges are based on selected figures from the original articles. To peruse the full range of systems the model were validated for, the user is directed to the original article.

Finally, for systems containing Fe, the correct ratio of Fe(II) and Fe(III) has to be provided. This means the user needs to know the oxidation environment of the system, and from that estimate this ratio before passing it on to the model.

5.1.3 Model Formulation

This model is based on the work of Thibodeau (2016). It estimates the total electrical conductivity, assuming it to be equal to the total ionic conductivity, by calculating the sum of the contributions from each cationic species, as shown in Equation (5.1).

$$\sigma = \sum_i \sigma_i \quad (5.1)$$

For each cationic species, electrical conductivity is defined as per Equation (5.2), indicating a dependence on molar volume and diffusivity;

$$\sigma_i = \frac{n_i x_i z_i^2 F^2}{\bar{V} RT} D_i \quad (5.2)$$

The molar volume and diffusion coefficient values are obtained from the models described in Chapter 4 and Chapter 6, respectively.

5.1.4 Assumptions

Equation (5.2) makes several assumptions.

1. It assumes that all cations are available to carry charge, meaning there are no neutral species or complexes.
2. It is assumed that the mechanism for ionic conductivity is the same as tracer diffusion.
3. It assumes that the velocity of an ion is determined solely by the forces acting on that specific ion. Thus, the electric field does not influence the medium through which the cations diffuse.

5.1.5 Literature Inaccuracies

The contour mapping of electrical conductivity shown in Thibodeau (2016) Figure 34 is likely incorrect. [auxi-mpp](#) were successfully validated against all Cartesian plots in Thibodeau (2016), but could not reproduce their contour mapping – see Figure 5.4. Figure 5.4a shows all composition slices for which [auxi-mpp](#) were successfully validated, yet the contour plot for $\text{Al}_2\text{O}_3 - \text{CaO} - \text{SiO}_2$ differs. Single point calculations for several selected compositions on Figures 5.4b to 5.4c also consistently agreed with [auxi-mpp](#)'s contour mapping. Finally, the same method to create the ternary plots in Figure 5.4 were used to create those in Figure 4.5 where there were no issues.

5.1.6 Model Validation

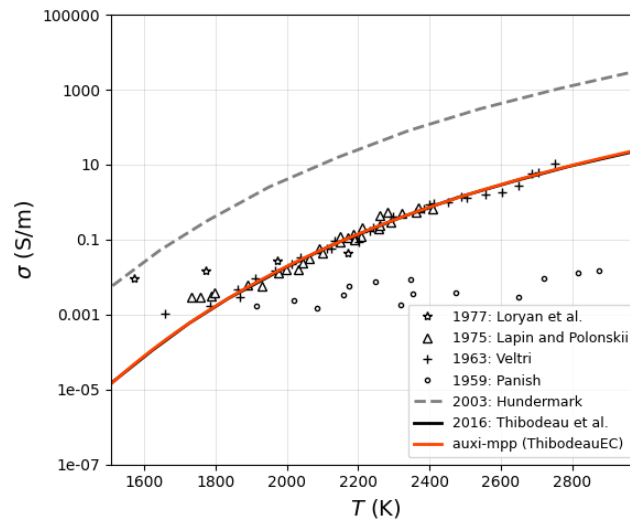
The Thibodeau electrical conductivity (ThibodeauEC) model implemented in [auxi-mpp](#) was validated against the literature model and experimental data extracted from Thibodeau (2016). The systems and temperatures for which the models were validated are given in Table 5.1.

Table 5.1: Electrical Conductivity Validation Ranges

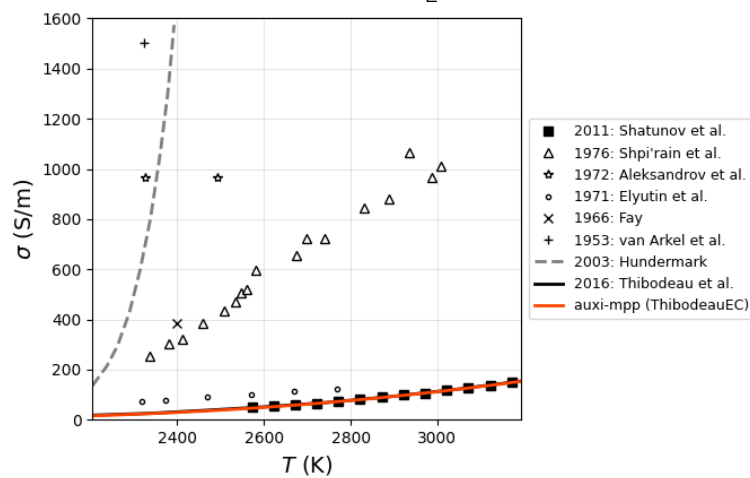
Model	Systems	Composition	Temperature (K)
Unary	SiO ₂	pure substance	1500 – 3000
	Al ₂ O ₃	pure substance	2200 – 3200
	MgO	pure substance	2000 – 3400
	CaO	pure substance	1800 – 3400
Binary	Al ₂ O ₃ – SiO ₂	$x_{\text{Al}_2\text{O}_3} = 0 - 1$	1873, 1973, 2073
	CaO – SiO ₂	$x_{\text{CaO}} = 0.2 - 0.7$	1823, 1873, 1923
	MgO – SiO ₂	$x_{\text{MgO}} = 0.2 - 0.8$	1873, 1973, 2073
Ternary	Al ₂ O ₃ – CaO – SiO ₂	$y_{\text{Al}_2\text{O}_3} = 0 - 1, y_{\text{CaO}}/y_{\text{SiO}_2} = 1$	1673, 1773, 1873
	Al ₂ O ₃ – CaO – SiO ₂	$y_{\text{CaO}} = 0 - 0.9, y_{\text{SiO}_2} = 0.1$	1673, 1773, 1873
	Al ₂ O ₃ – CaO – SiO ₂	$y_{\text{CaO}} = 0 - 0.8, y_{\text{SiO}_2} = 0.2$	1673, 1773, 1873
	Al ₂ O ₃ – CaO – SiO ₂	$y_{\text{CaO}} = 0 - 0.7, y_{\text{SiO}_2} = 0.3$	1673, 1773, 1873
	Al ₂ O ₃ – CaO – SiO ₂	$y_{\text{CaO}} = 0 - 0.6, y_{\text{SiO}_2} = 0.4$	1673, 1773, 1873
	Al ₂ O ₃ – CaO – SiO ₂	$y_{\text{CaO}} = 0 - 0.95, y_{\text{Al}_2\text{O}_3} = 0.05$	1673, 1773, 1873
	Al ₂ O ₃ – CaO – SiO ₂	$y_{\text{CaO}} = 0 - 0.9, y_{\text{Al}_2\text{O}_3} = 0.1$	1673, 1773, 1873
	Al ₂ O ₃ – CaO – SiO ₂	$y_{\text{CaO}} = 0 - 0.8, y_{\text{Al}_2\text{O}_3} = 0.2$	1673, 1773, 1873
	Al ₂ O ₃ – MgO – SiO ₂	$y_{\text{MgO}} = 0 - 0.5, y_{\text{SiO}_2} = 0.5$	1873, 1973, 2073
	CaO – MgO – SiO ₂	$x_{\text{MgO}} = 0 - 0.4, x_{\text{CaO}}/x_{\text{SiO}_2} = 1$	1773, 1823, 1873
	Al ₂ O ₃ – CaO – SiO ₂ [‡]	$y_{\text{Al}_2\text{O}_3, \text{CaO}, \text{SiO}_2} = 0 - 1$	1873
	CaO – MgO – SiO ₂ [‡]	$y_{\text{CaO}, \text{MgO}, \text{SiO}_2} = 0 - 1$	1873
Quaternary [‡]	Al ₂ O ₃ – CaO – MgO – SiO ₂	$y_{\text{CaO}, \text{MgO}, \text{SiO}_2} = 0 - 0.9, y_{\text{Al}_2\text{O}_3} = 0.1$	1873
	Al ₂ O ₃ – CaO – MgO – SiO ₂	$y_{\text{Al}_2\text{O}_3, \text{CaO}, \text{SiO}_2} = 0 - 0.9, y_{\text{MgO}} = 0.1$	1873

[‡] See Figure 5.4

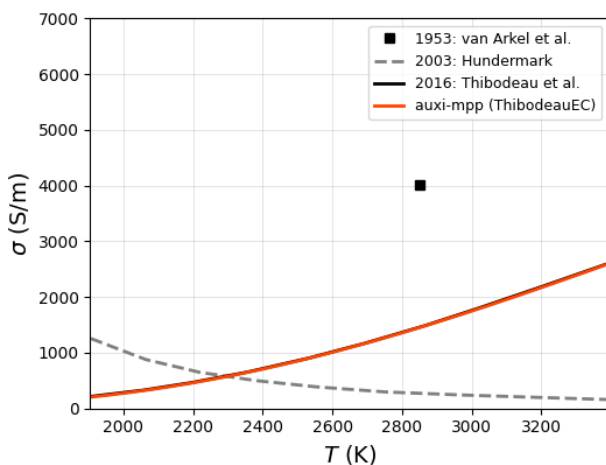
[auxi-mpp](#)'s ThibodeauEC model closely reproduces the literature model, which itself shows good agreement with experimental data (Thibodeau 2016). See Figures 5.1 to 5.3 for model performance for unary, binary and ternary systems.



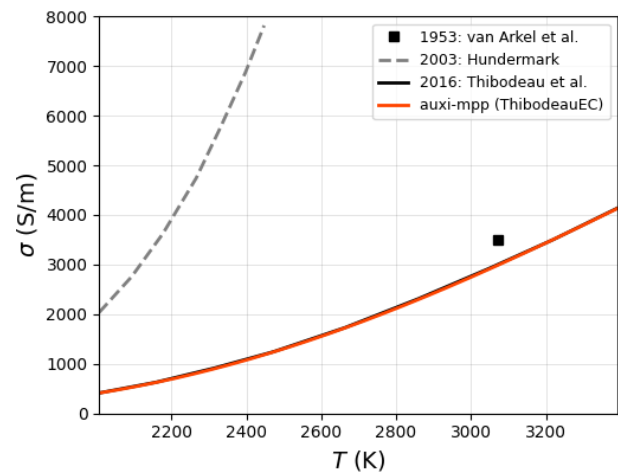
(a) SiO_2



(b) Al_2O_3



(c) CaO



(d) MgO

Figure 5.1: Electrical conductivity vs temperature for unary systems.

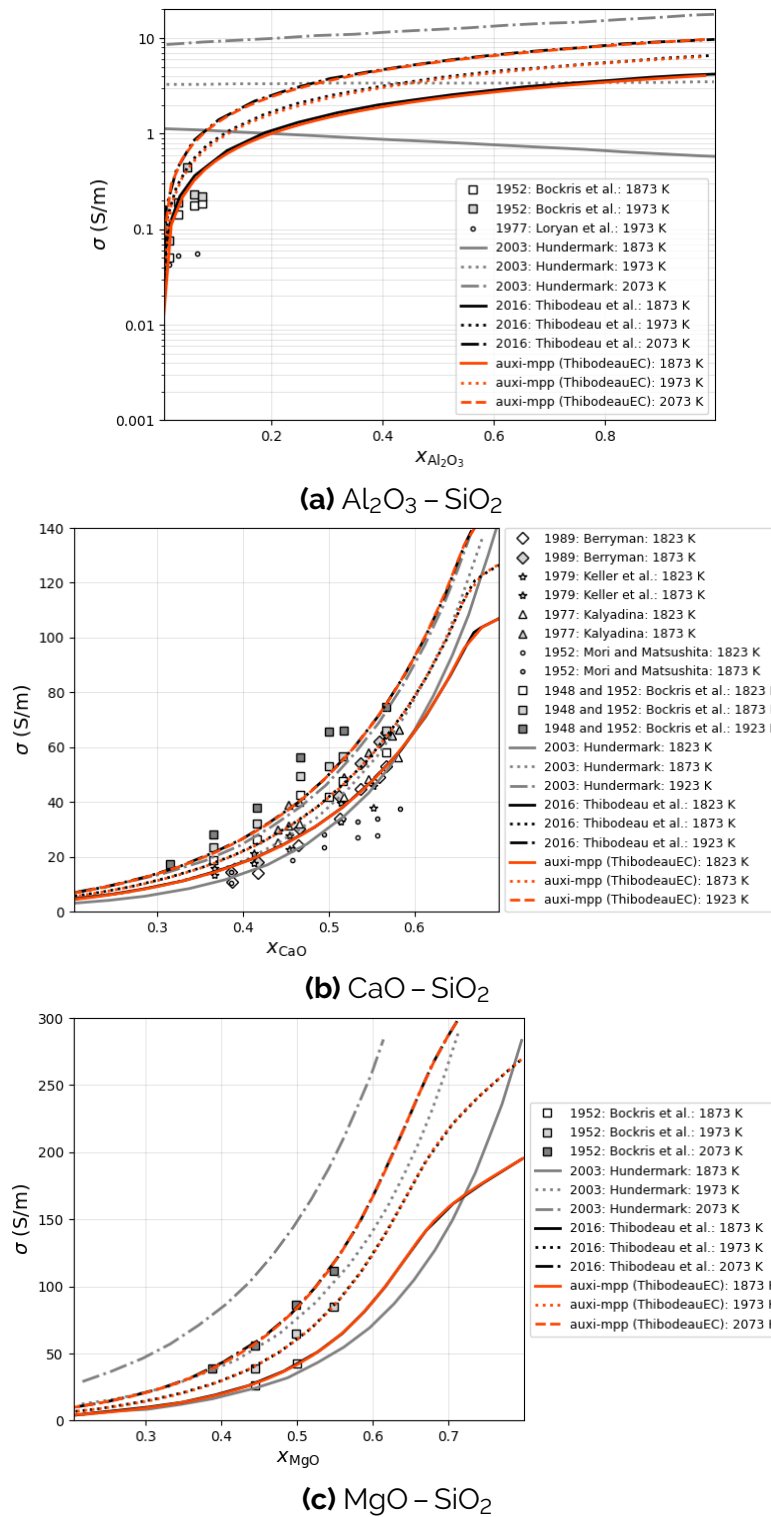
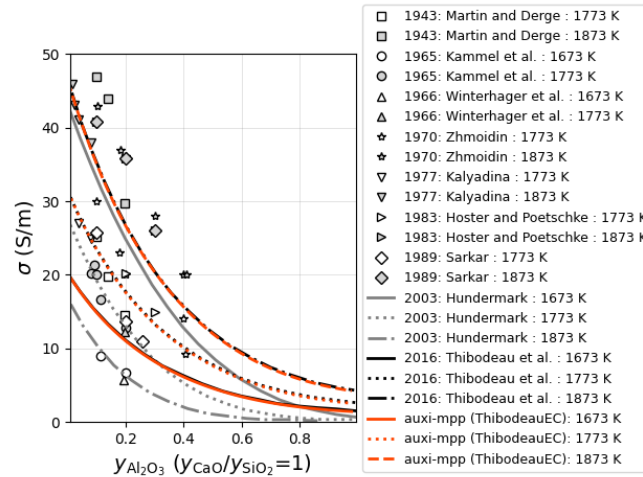
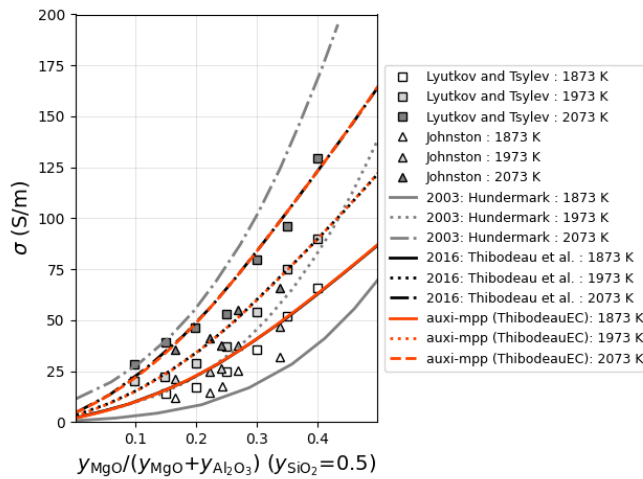


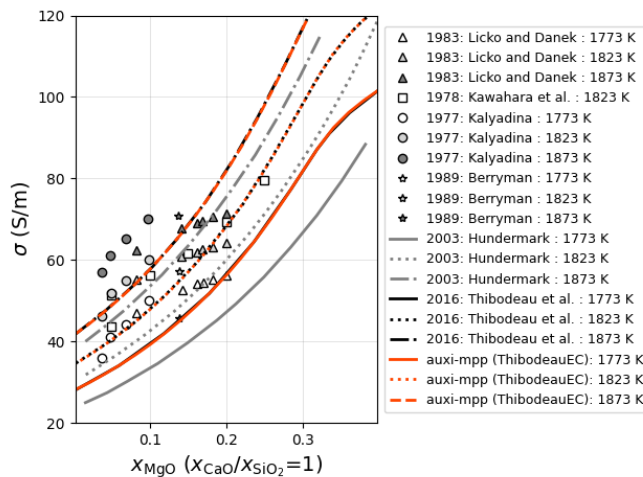
Figure 5.2: Electrical conductivity vs mole fraction of binary systems.



(a) $\text{Al}_2\text{O}_3 - \text{CaO} - \text{SiO}_2$



(b) $\text{Al}_2\text{O}_3 - \text{MgO} - \text{SiO}_2$



(c) $\text{CaO} - \text{MgO} - \text{SiO}_2$

Figure 5.3: Electrical conductivity vs mole fraction of ternary systems.

When reproducing the contour mapping of electrical conductivity for ternary and quaternary systems, as shown in Figure 5.4, there is not an exact agreement with literature, however.

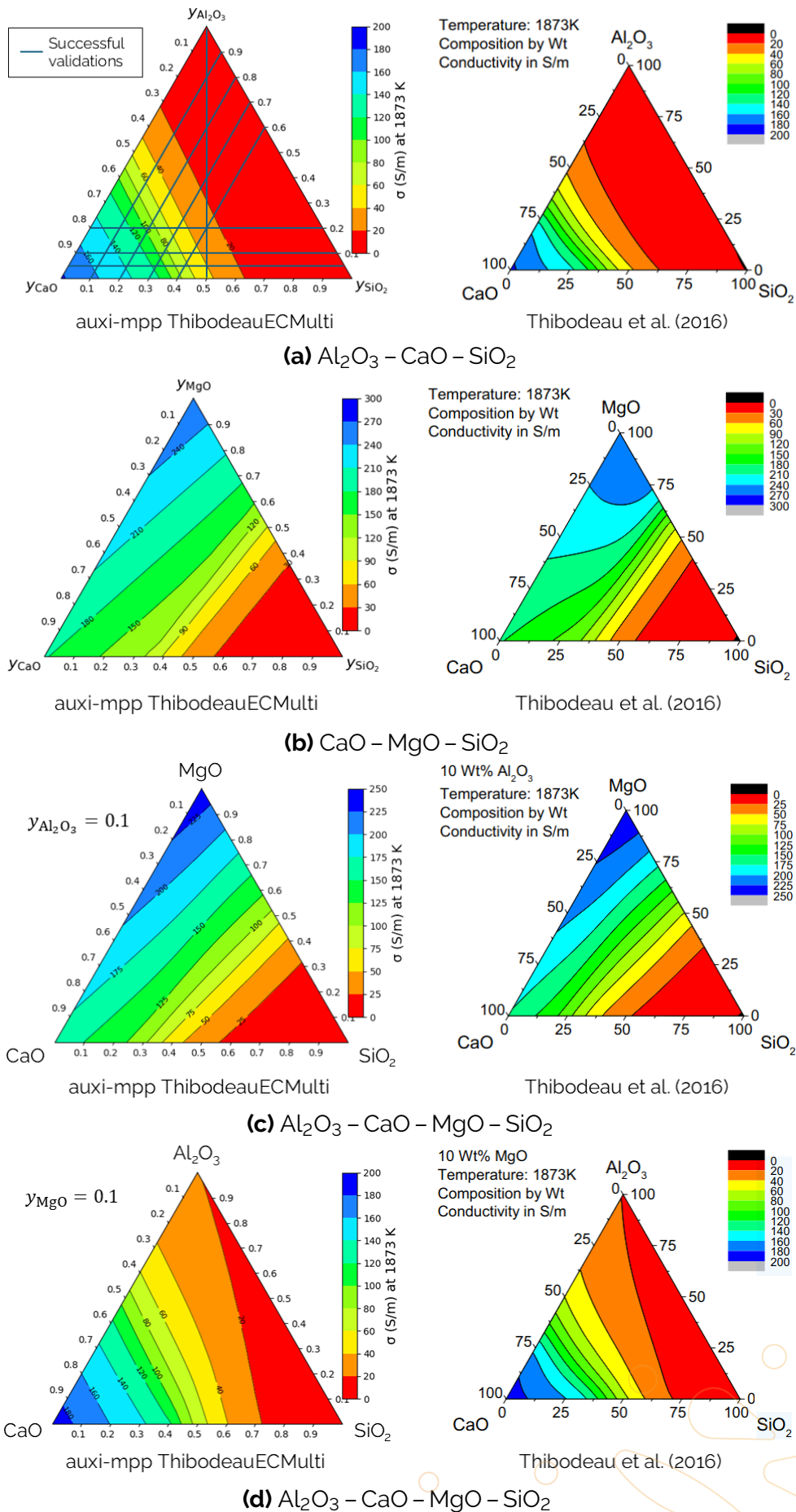


Figure 5.4: Comparing **auxi-mpp**'s contour mapping of electrical conductivity with literature

We believe this to be a mistake in the literature plots for a few good reasons. Figure 5.4a shows all composition slices for which the model were successfully validated against Thibodeau's own figures. There were no Cartesian plot in Thibodeau (2016) that [auxi-mpp](#) could not reproduce. Secondly, the method used to create the plots could exactly reproduce the contour mapping for ternary and quaternary systems for molar volume – see Figure 4.5. This also confirms that there are no issues with the bond fractions used. Finally, calculations performed on selected points in Figures 5.4b to 5.4d consistently agreed with [auxi-mpp](#)'s mapping. Nevertheless, the contour mappings are relatively close to that in literature.

Issues

There are no current issues with this model.

5.2 Hundermark Electrical Conductivity Models

Models developed by Hundermark (2003).

5.2.1 Introduction

The unified model for estimating the electrical conductivity of melter-type slags, developed by Hundermark (2003), originated from challenges in the electrical control of furnaces used by South African platinum producers. The initial design was an iron-free model for Al_2O_3 – CaO – MgO – SiO_2 slags, based on the principle of ionic conduction as the sole operating mechanism. This foundational work was later integrated with data from iron-containing systems to create the comprehensive unified model.

5.2.2 Model Overview

Hundermark's unified model estimates the electrical conductivity of melter-type slags based on their composition, temperature, and oxidation state (Hundermark 2003). It is applicable to slags containing two or more of the following components: Al_2O_3 , CaO , FeO_x , MgO , and SiO_2 . The model is particularly useful for Fe-bearing slags where other models, like Thibodeau's, have shown to be unreliable (Thibodeau 2014). While empirical, the model provides reasonably accurate estimates for a wide range of slag systems, achieving an average correlation coefficient of 0.9743 with experimental values.

The model was developed by integrating two separate datasets. The first part was a foundational Fe-free model for the Al_2O_3 – CaO – MgO – SiO_2 system represented by Equation (5.3). This initial model, which assumed that ionic conduction is the sole mechanism, used multiple linear regressions to correlate slag composition with conductivity, yielding a correlation coefficient of 0.8358 for temperatures between 1623 to 2023 K.

The second part incorporated data from Fe-containing systems. By combining both datasets, the unified model, represented by eq. (5.4), explicitly accounts for the fractions of ferrous (Fe^{2+}) and ferric (Fe^{3+}) ions, allowing it to estimate conductivity changes with varying slag oxidation states.

It is important to note that this model is formulated strictly for liquid slag systems – the user should therefore ensure that his/her system is above the liquidus temperature before performing calculations. Also, we recommend the model to be used within the validation ranges specified in Table 5.2. The validation ranges are based on selected figures from the original articles. To peruse the full range of systems the model were validated for, the user is directed to the original article.

Finally, for systems containing Fe, the correct ratio of Fe(II) and Fe(III) has to be provided. This means the user needs to know the oxidation environment of the system, and from that estimate this ratio before passing it on to the model.

5.2.3 Model Formulation

The model formulation is the foundational Fe-free model is given by Equation (5.3), while the unified model, which includes the contribution of ferrous and ferric ions, is repre-

sented by Equation (5.4).

$$\ln \sigma = \left(31.6 - \frac{68048}{T} \right) x_{\text{Al}_2\text{O}_3} + \left(-2.2 - \frac{9006}{T} \right) x_{\text{CaO}} + \left(10.5 - \frac{15049}{T} \right) x_{\text{MgO}} + \left(17.1 - \frac{40544}{T} \right) x_{\text{SiO}_2} \quad (5.3)$$

$$\ln \sigma = \left(19.9 - \frac{47348}{T} \right) x_{\text{Al}_2\text{O}_3} + \left(15.4 - \frac{24087}{T} \right) x_{\text{CaO}} + \left(9.2 - \frac{14151}{T} \right) x_{\text{MgO}} + \left(-0.5 - \frac{7478}{T} \right) x_{\text{SiO}_2} + \left(10.0 - \frac{9140}{T} \right) x_{\text{FeO}_x} \cdot x_{\text{Fe}^{2+}} + \left(65.4 - \frac{82447}{T} \right) x_{\text{FeO}_x}^2 \cdot x_{\text{Fe}^{2+}} \cdot x_{\text{Fe}^{3+}} + \left(-2.6 + \frac{6642}{T} \right) x_{\text{FeO}_x} \cdot x_{\text{Fe}^{3+}} \quad (5.4)$$

Where σ represents the electrical conductivity, with units of S cm^{-1} , x_i is the mole fraction of component i , and T is the temperature in Kelvins. x_{FeO_x} is the equivalent mole fraction of the total ferrous and ferric oxide in the slag, while $x_{\text{Fe}^{2+}}$ and $x_{\text{Fe}^{3+}}$ refer to the ferrous and ferric fractions, respectively.

5.2.4 Assumptions

Several assumptions were made in the development of the Hundermark model, which are important to consider when applying the model. These assumptions include:

1. A primary assumption for the Fe-free model is that ionic conduction is the only mechanism operating in these Fe-free systems and it results solely from the movement of cations like Mg^{2+} and Ca^{2+} .
2. The Fe-free model assumes that the temperature dependence of the conductivity obeys the Arrhenius relationship. Furthermore, it was observed and incorporated into the model that the activation energy for conduction and the natural logarithm of the pre-exponential factor are linearly related, following a compensation law.
3. The Fe-free model is specifically developed for slags containing Al_2O_3 , CaO , MgO , and SiO_2 in a temperature range of 1623 to 2023 K.
4. The models are fundamentally semi-empirical, meaning they are based on observed relationships and regressions techniques rather than being derived purely from first principles of slag structure or ion transport mechanisms.
5. The unified model is specifically designed for slags containing two or more of Al_2O_3 , CaO , FeO_x , MgO , and SiO_2 components, and a temperature range of 1623 to 2023 K.
6. Only electrical conductivity data for fully molten slags (above their liquidus temperature) were considered for the models' development to avoid inconsistencies arising from the presence of solid phases.

5.2.5 Model Validation

Hundermark's, Fe-free, electrical conductivity model, implemented in [auxi-mpp](#), was validated against literature model data and experimental data extracted from Thibodeau (2016) and Thibodeau (2014), as Hundermark (2003) did not contain such plots for validation. The systems and temperatures for which the models were validated are given in Table 5.2.

Table 5.2: Electrical Conductivity Validation Ranges

Model	Systems	Composition	Temperature (K)
Unary	SiO ₂	pure substance	1500 – 3000
	MgO	pure substance	2000 – 3400
	CaO	pure substance	1800 – 3400
	CaO – SiO ₂	$x_{\text{CaO}} = 0.2 - 0.7$	1823, 1873, 1923
	MgO – SiO ₂	$x_{\text{MgO}} = 0.2 - 0.8$	1873, 1973, 2073
Ternary	CaO – MgO – SiO ₂	$x_{\text{MgO}} = 0 - 0.4, x_{\text{CaO}}/x_{\text{SiO}_2} = 1$	1773, 1823, 1873

For Fe-free systems, [auxi-mpp](#)'s implementation of Hundermark's Fe-free model closely reproduces the literature model for all but accept systems containing Al₂O₃ (Thibodeau 2014). See Figures 5.5 to 5.7 for model performance for unary, binary and ternary systems.

For the Fe-bearing system in Figure 5.8, Hundermark's unified model in [auxi-mpp](#) was used to estimate the electrical conductivity value. It is clearly evident from Figure 5.8 that the [auxi-mpp](#) estimates are not the same as Hundermark's extracted model data. In later updates this will be investigated further and additional validation plots for Fe-bearing systems will be added.

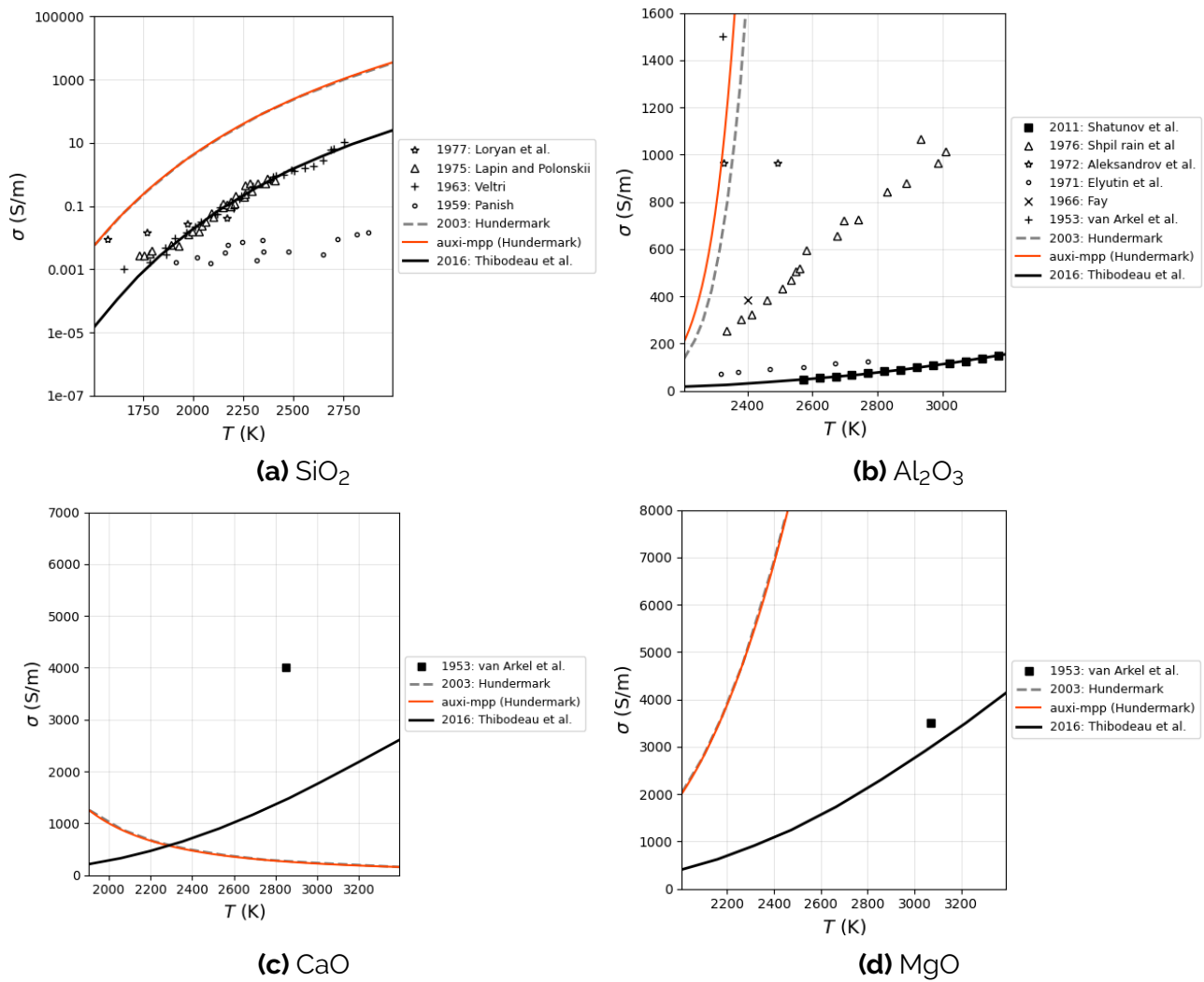
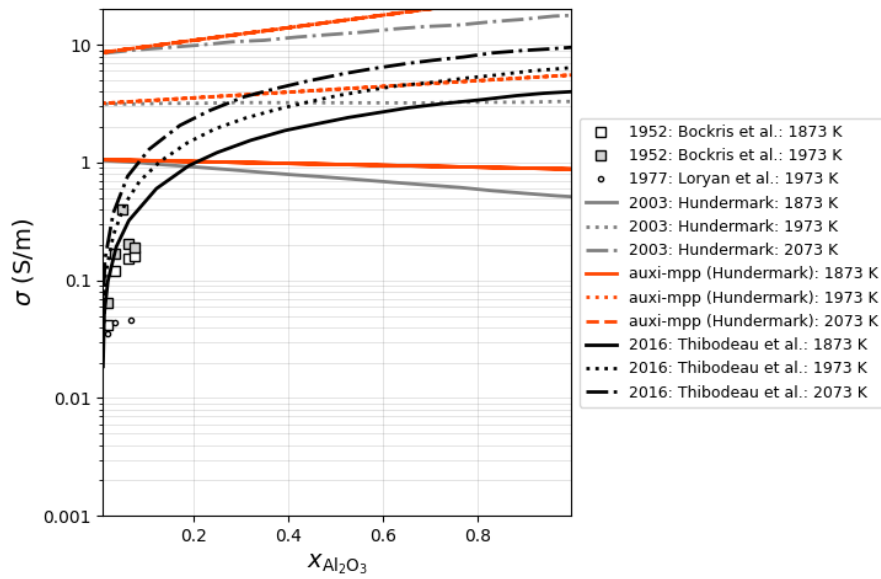
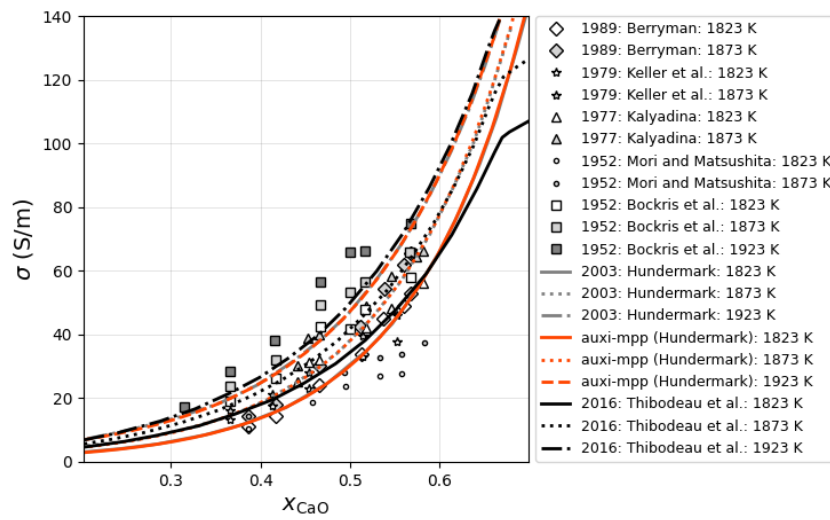


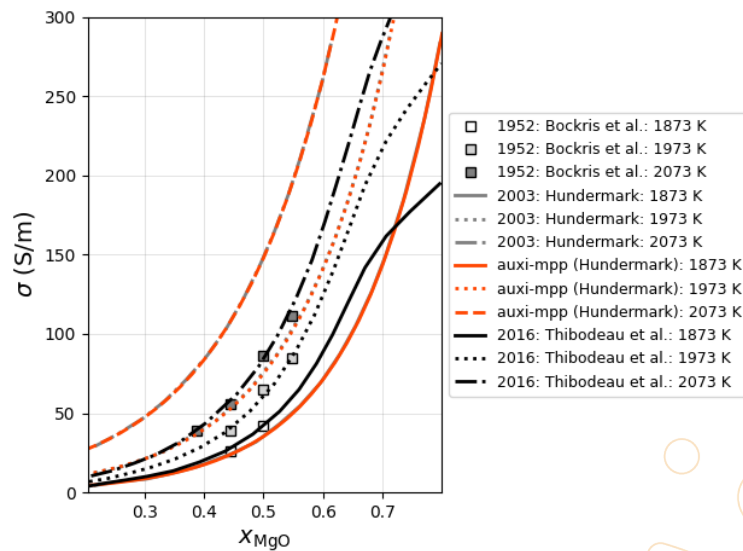
Figure 5.5: Electrical conductivity vs temperature for unary systems.



(a) $\text{Al}_2\text{O}_3 - \text{SiO}_2$

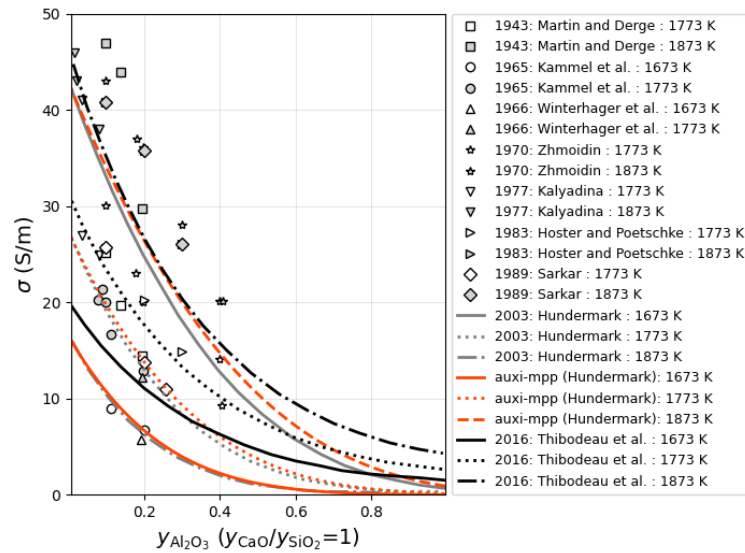


(b) $\text{CaO} - \text{SiO}_2$

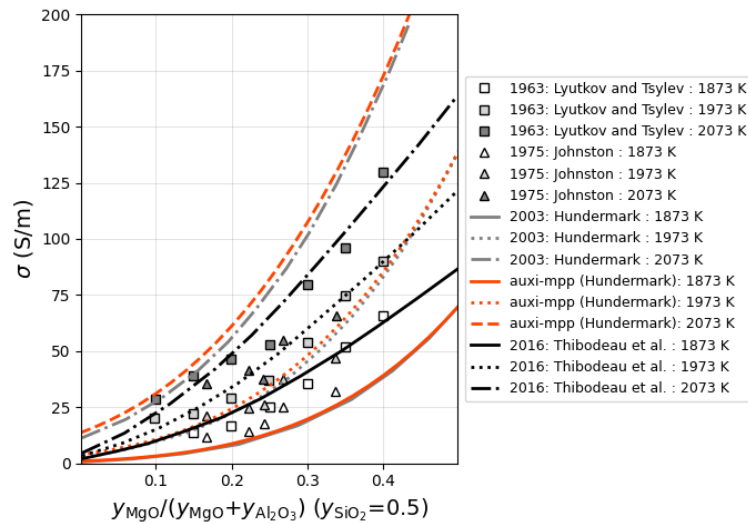


(c) $\text{MgO} - \text{SiO}_2$

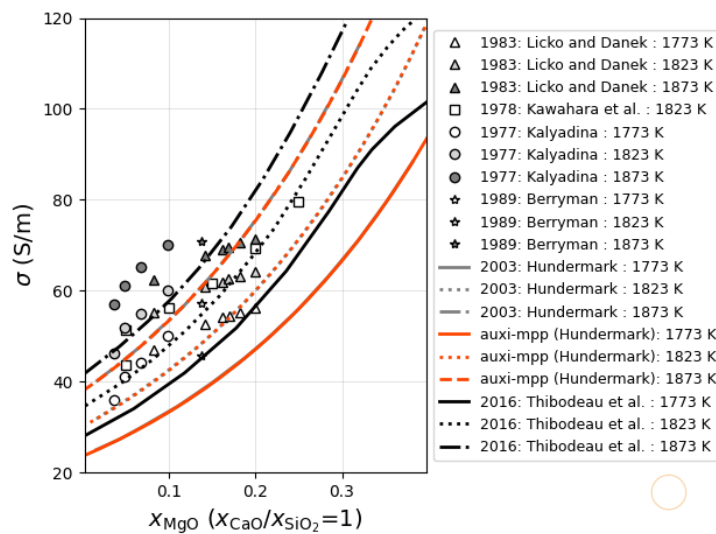
Figure 5.6: Electrical conductivity vs mole fraction of binary systems.



(a) $Al_2O_3 - CaO - SiO_2$



(b) $Al_2O_3 - MgO - SiO_2$



(c) $CaO - MgO - SiO_2$

Figure 5.7: Electrical conductivity vs mole fraction of ternary systems.

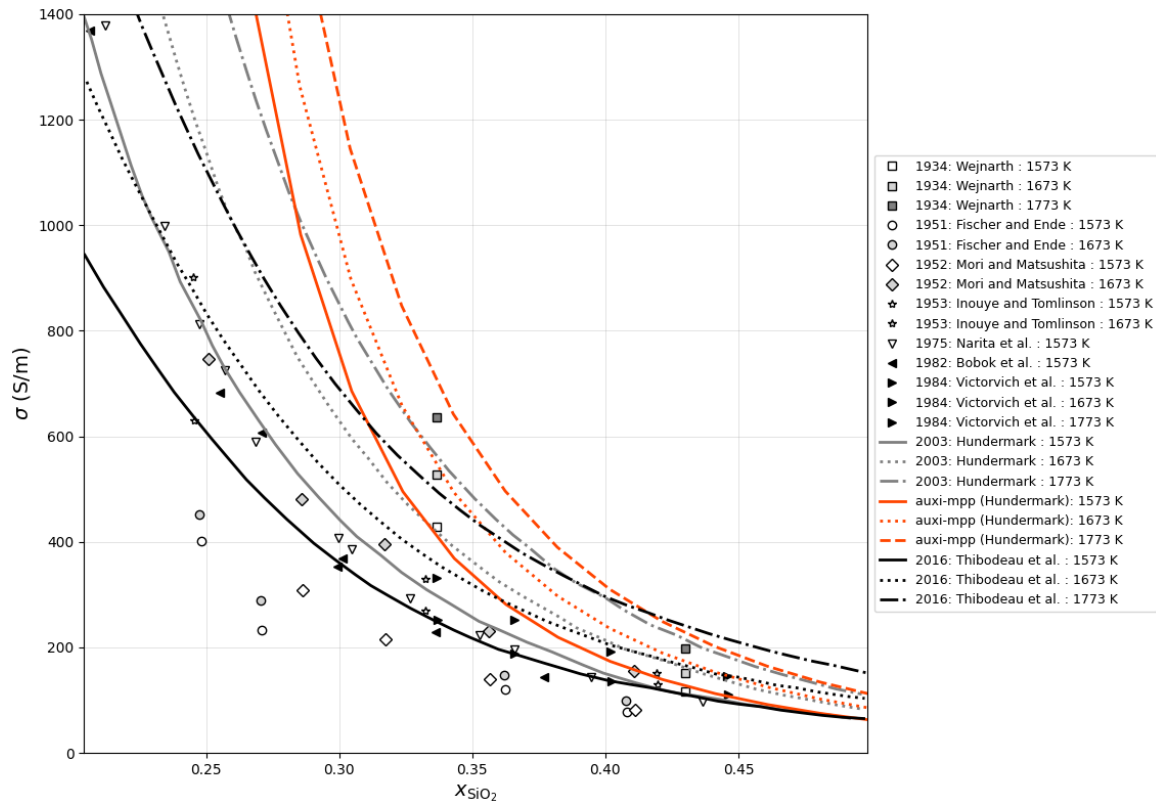


Figure 5.8: Electrical conductivity vs mole fraction for FeO – Fe₂O₃ – SiO₂ system.

Issues

Systems containing Al₂O₃ could not be validated. Despite the agreement of the implemented parameters of Al₂O₃ with literature, [auxi-mpp's Hundermark \(2003\)](#) model could not replicate the electrical conductivity for systems containing Al₂O₃, as reported by [Thibodeau et al. \(2016a\)](#).

The electrical conductivity could also not be replicated for the FeO – Fe₂O₃ – SiO₂ system.

These issues will be investigated in the future.

Chapter 6

Diffusivity

6.1 Thibodeau Diffusivity Model

A model implemented by Thibodeau (2016).

6.1.1 Introduction

As with all physical properties, the diffusivity is also affected by the structure of the slag. The higher the polymerisation, the more rigid the slag structure and therefore the more difficult particles will diffuse through it. A model that calculates diffusivity (diffusion coefficients) from slag polymerisation is thus presented here.

6.1.2 Model Overview

Variations in slag composition affecting polymerisation are accounted for using bond fractions, calculated with the MQM model in [ChemApp for Python](#) and data from [FactSage's FToxid database](#). The model's parameters for individual cations are determined using data from unary and binary silicate systems, and is capable of estimating the electrical conductivity of higher-order systems without additional parameters.

The bond fractions with the model parameters are then used to scale the activation energy that dictates the rate of diffusion. This is done in an Arrhenius-like equation which is similar to Equation (6.1). Arrhenius-like equations are typically used to calculate temperature dependence for reaction rates.

$$D = A \exp \left(-\frac{E}{RT} \right) \quad (6.1)$$

It is important to note that this model is formulated strictly for liquid slag systems – the user should therefore ensure that his/her system is above the liquidus temperature before performing calculations. Finally, for systems containing Fe, the correct ratio of Fe(II) and Fe(III) has to be provided. This means the user needs to know the oxidation environment of the system, and from that estimate this ratio before passing it on to the model.

6.1.3 Model Formulation

The diffusivity used in the calculation of the electrical conductivity described in Equation (5.2), is determined in Equation (6.2) with parameters for systems containing network formers such as SiO_2 and Al_2O_3 .

$$D_i = A_i \exp \left(- \frac{B_i + C_{i-\text{SiSi}} x_{\text{Si-Si}} + C_{i-\text{SiAl}} x_{\text{Si-Al}} + C_{i-\text{AlAl}} x_{\text{Al-Al}}}{RT} \right) \quad (6.2)$$

The bond fractions (x_{i-j}) calculated from the MQM model are combined with the parameters A_i , B_i , and C_i from Thibodeau (2016).

This model is limited to the following cations; Mg^{2+} , Ca^{2+} , Mn^{2+} , Pb^{2+} , Fe^{2+} , Fe^{3+} , Al^{3+} , and Si^{4+} .

6.1.4 Variable Declarations

The parameters used in the model are extracted from Thibodeau (2014) and are given in Table 6.1.

Table 6.1: Electrical Conductivity Parameters (Thibodeau 2014)

	A_i ($\text{cm}^2 \text{s}^{-1}$)	B_i (kJ mol^{-1})	$C_{i-\text{SiSi}}$ (kJ mol^{-1})	$C_{i-\text{AlAl}}$ (kJ mol^{-1})	$C_{i-\text{AlSi}}$ (kJ mol^{-1})
Mg^{2+}	0.03448	118.6	42.1	10.0	10.0
Ca^{2+}	0.02600	115.0	35.0	35.0	35.0
Mn^{2+}	0.05421	104.2	55.4	20.0	20.0
Pb^{2+}	0.00936	65.4	90.4	90.4	90.4
Fe^{2+}	0.04200	95.0	-	-	-
Fe^{3+}	0.00358	158.3	-	-	-
Al^{3+}	0.00358	158.3	-	-	-
Si^{4+}	5.22600	380.9	-	-	-

6.1.5 Assumptions

In this diffusivity model, the following assumptions were made.

1. It is assumed that the activation energy of the ionic conductivity is linearly increasing with the bond fractions of Si – Si and Al – Al.
2. It is assumed that that $C_{i-\text{SiAl}}$ will be equal to $C_{i-\text{AlAl}}$, instead of the average between $C_{i-\text{AlAl}}$ and $C_{i-\text{SiSi}}$. This is because it will be significantly more likely for the cations to take the lower energy route, which is on the Al side of the bond.
3. It is assumed that Al_2O_3 behaves like a network former, despite its amphoteric behaviour.
4. Parameters for Fe^{3+} were fixed to the same values as Al^{3+} as there was no data available capable of providing a better first estimate.

6.1.6 Simplifications

For applying Equation (6.2), interactions between diffusing network modifier cations are neglected. This simplifies the model, allowing it to estimate diffusion coefficients of higher-order systems from unary and binary parameters without additional parameters.

6.1.7 Model Validation

This model is not independently used or implemented due to lack of literature data for comparison. However, Chapter 5's electrical conductivity estimates incorporate the diffusivity model's results. This model was successfully validated and thereby indirectly validates the diffusivity model.

Chapter 7

Viscosity

7.1 Grundy-Kim-Brosch Viscosity Model

Model developed by Grundy et al. (2008b), Grundy et al. (2008b), Kim (2011), and Brosh et al. (2012).

7.1.1 Introduction

The Grundy-Kim-Brosch viscosity model, which accounts for silicate structure estimated using the MQM model with ChemApp for Python and the FactSage FToxid database, is currently implemented for unary through multi component systems containing SiO₂, CaO, MgO, Al₂O₃, FeO and Fe₂O₃.

7.1.2 Model Overview

The principle equation implemented in the model to calculate the viscosity (μ) for a slag is an Arrhenius-like equation, Equation (7.1). It is a function of both temperature and composition where μ is the viscosity in Pa s, R is the gas constant and T is the temperature in Kelvin.

$$\ln(\mu) = A + \frac{E}{RT} \quad (7.1)$$

The parameters A and E depends on the slag composition. For unary systems the compound specific A and E parameters are simply plugged into Equation (7.1) together with the system temperature. However, with silicate binary or multicomponent systems, A and E are not only determined by the pure substance character, but also by the interaction between the components and by the degree of polymerisation.

It is important to note that this model is formulated strictly for liquid slag systems – the user should therefore ensure that his/her system is above the liquidus temperature before performing calculations. Also, we recommend the model to be used within the validation ranges specified in Table 7.3 and Figure 7.8. The validation ranges are based on selected figures from the original articles. To peruse the full range of systems the model were validated for, the user is directed to the original article.

Finally, for systems containing Fe, the correct ratio of Fe(II) and Fe(III) has to be provided. This means the user needs to know the oxidation environment of the system, and from that estimate this ratio before passing it on to the model.

7.1.3 Unary and Binary Model Formulation

Unary Model

For unary systems, Equation (7.1) is used directly, where A and E are unique to each component. For systems containing two or more components, the structure of the slag becomes more complex, requiring A and E to be estimated based on several structural contributions.

Binary Model

Starting with the Arrhenius-like equation, Equation (7.1), instead of using a single parameter for A and E , these are weighted based on different structural contributions. For binary systems, A is calculated as in Equation (7.2);

$$A = A_M x_M^{s_0} + x_{Si}^{s_0} [A_{SiO_2}^* + A_{SiO_2}^E p^{40} + A_{M-Si} x_M^{s_0} + A_{M-Si}^R (p^4 - p^{40})] \quad (7.2)$$

and E is calculated as in Equation (7.3);

$$E = E_M x_M^{s_0} + x_{Si}^{s_0} [E_{SiO_2}^* + E_{SiO_2}^E p^{40} + E_{M-Si} x_M^{s_0} + E_{M-Si}^R (p^4 - p^{40})] \quad (7.3)$$

where p is a probability factor used to estimate the degree of polymerisation in the system, and is calculated in Equation (7.4).

Estimating Polymerisation

Silicate melt structure is defined by the bridging behaviour of oxygen atoms, influencing the polymerisation of SiO_4 tetrahedra into three-dimensional networks. The degree of polymerisation, quantified by the average number of bridging oxygens around silicon, can be estimated from bond fractions calculated using the MQM. The first step to estimate the degree of polymerisation is to know the probability for a given Si atom to form one Si-Si bridge. This probability is given by p in Equation (7.4).

$$p = \frac{2n_{Si-Si}}{2n_{Si-Si} + \sum_M n_{Si-M}} \quad (7.4)$$

$$= \frac{x_{Si-Si}}{2x_{Si-Si} + \sum_M x_{Si-M}} \quad (7.5)$$

As a first approximation, p can be calculated by dividing the total number of Si-Si bridges from all silicon atoms by the combined total of Si-Si and Si-M bridges. Each Si-Si bridge is counted twice since an O° bond emanates from each silicon atom in the bridge.

The probability that a given silicon atom is a Q^4 -species is p^4 , as this atom is connected to four Si – Si bridges. This principle extends to Si – Si bridges forming chains. The probability of encountering m Si – Si bridges connected to form a chain of length m is proportional to p^m .

Thus, p^m , where m is a natural number, serves as a measure of the abundance of various Si – Si cluster sizes present in the slag (Kim et al. 2012a). A critical cluster size can be defined to represent the formation of a percolating SiO_2 network. Once this cluster size is reached, the μ increases dramatically. Analysis of the viscosity data suggests that a cluster of 40 interconnected Si – Si pairs is an appropriate choice for the critical cluster size (Kim et al. 2012a).

7.1.4 Multicomponent Model Formulation

Systems Without Alumina

For the implemented model, both A and E are functions of slag composition, x , and are expressed in terms of multiple additional contributing parameters shown in Equation (7.6) and Equation (7.7). These equations provide estimates for A and E for unary, binary, and multi-component systems, with the primary constraint of having the appropriate optimised binary parameters to describe the system of interest. As indicated by Equation (7.6) and Equation (7.7), each individual parameter within these equations are multiplied with ionic compositions of $x_{\text{Si}}^{s_0}$ or $x_{\text{M}}^{s_0}$ to account for their contributions to the overall viscosity of the slag.

Therefore, it is important to note that the input compositions that are generally expressed with the formulas of the oxide components, need to be converted to ionic compositions ($x_{\text{SiO}_2}^{s_f} \rightarrow x_{\text{Si}}^{s_0}$) to be used in the model.

$$A = \sum_{\text{M=Na,Ca,Mg,...}} A_{\text{M}} x_{\text{M}}^{s_0} + A_{\text{Si}}^* x_{\text{Si}}^{s_0} + A_{\text{Si}}^E x_{\text{Si}}^{s_0} p^{40} + \sum_{\text{M}} A_{\text{M-Si}} x_{\text{M}}^{s_0} x_{\text{Si}}^{s_0} + x_{\text{Si}}^{s_0} (p^4 - p^{40}) \times \sum_{\text{M}} A_{\text{M-Si}}^R \frac{x_{\text{M}}^{s_0}}{\sum_{\text{M}} x_{\text{M}}^{s_0}} \quad (7.6)$$

$$E = \sum_{\text{M=Na,Ca,Mg,...}} E_{\text{M}} x_{\text{M}}^{s_0} + E_{\text{Si}}^* x_{\text{Si}}^{s_0} + E_{\text{Si}}^E x_{\text{Si}}^{s_0} p^{40} + \sum_{\text{M}} E_{\text{M-Si}} x_{\text{M}}^{s_0} x_{\text{Si}}^{s_0} + x_{\text{Si}}^{s_0} (p^4 - p^{40}) \times \sum_{\text{M}} E_{\text{M-Si}}^R \frac{x_{\text{M}}^{s_0}}{\sum_{\text{M}} x_{\text{M}}^{s_0}} \quad (7.7)$$

Background to these individual parameters is given as follows.

The parameters A_{M} and E_{M} are the contributions to the viscosity of the pure liquid oxides MO_x , Equation (7.8). These are non-network formers.

$$\ln \mu_{\text{MO}_x} = A_{\text{M}} + \frac{E_{\text{M}}}{RT} \quad (7.8)$$

Similarly, Equation (7.9), describes the hypothetical viscosity of SiO_2 if it behaved as a basic oxide and did not form a network.

$$\ln \mu_{\text{SiO}_2}^* = A_{\text{Si}}^* + \frac{E_{\text{Si}}^*}{RT} \quad (7.9)$$

The excess contribution per Si atom from large clusters of Q^4 -species, where a silicon atom is at the center of a group containing at least 40 interconnected Si – Si pairs, is proportional to p^{40} . This contribution is expressed through A_{Si}^E and E_{Si}^E . For a system with a composition of $x_{\text{Si}}^{S_0}$, the clustering effect is given by $x_{\text{Si}}^{S_0} \cdot p^{40}$, as shown in Equation (7.6) and Equation (7.7).

By combining the contributions of A_{Si}^E and E_{Si}^E with those of A_{Si}^* and E_{Si}^* , and assuming that the excess contributions of the silica network are independent of other cations M, the viscosity of pure SiO_2 can be calculated using Equation (7.10).

$$\ln \mu_{\text{SiO}_2} = (A_{\text{Si}}^* + A_{\text{Si}}^E) + \frac{(E_{\text{Si}}^* + E_{\text{Si}}^E)}{RT} \quad (7.10)$$

The excess contribution per Si atom from the remaining Q^4 -species, particularly from smaller clusters with fewer than 40 interconnected Si – Si pairs, is proportional to $(p^4 - p^{40})$. These smaller clusters, containing less than 40 Si – Si pairs, also affect viscosity and interact more directly with other oxides in the slag. The M cations are positioned closer to a given Si atom, making their contribution to viscosity system-dependent, and are combined with the binary parameters $A_{\text{M-Si}}^R$ and $E_{\text{M-Si}}^R$.

Finally, the binary parameters $A_{\text{M-Si}}$ and $E_{\text{M-Si}}$, are cross-terms used to account for small nonlinearities of the viscosity, if any, for binary systems M – Si and are therefore multiplied by the concentrations of both respective ions, $x_{\text{M}}^{S_0}$ and $x_{\text{Si}}^{S_0}$, associated with a binary oxide system.

The parameters A_{Si}^* , A_{Si}^E , E_{Si}^* and E_{Si}^E are properties of pure SiO_2 and so are common for all binary systems. $(A_{\text{Si}}^* + A_{\text{Si}}^E)$ and $(E_{\text{Si}}^* + E_{\text{Si}}^E)$ are equal to experimentally determined viscosity parameters A_{Si} and E_{Si} from pure SiO_2 .

The parameters $A_{\text{M-Si}}$, $E_{\text{M-Si}}$, $A_{\text{M-Si}}^R$ and $E_{\text{M-Si}}^R$ are characteristic of each binary system and are the only true binary viscosity parameters. The values for these parameters were optimised using critically evaluated experimental viscosity data. For binary systems studied, except for the $\text{AlO}_{1.5}$ – SiO_2 system, the parameters $A_{\text{M-Si}}$ and $A_{\text{M-Si}}^R$ were not required and are set to zero. The optimised parameters for the model are shown in Table 7.1 (Kim 2011; Kim et al. 2012b).

Systems Containing Al_2O_3 or Fe_2O_3

In the binary $\text{AlO}_{1.5}$ – SiO_2 system, Al^{3+} is assumed to be octahedrally coordinated by six oxygens, similar to its coordination in the aluminosilicate minerals mullite and sillimanite. In this state, Al^{3+} disrupts the silica network, forming non-bridging oxygens and acts as a network modifier, which lowers the viscosity of the silicate melt. However, in a melt containing both $\text{AlO}_{1.5}$ and MO_x , Al^{3+} can partially substitute for Si^{4+} in the silica network, acting as a network former. This substitution is possible as long as the network-forming Al^{3+} remains associated with the M^{1+} or M^{2+} ions that compensate for the missing charge. The same concept applies to Fe_2O_3 , where Fe^{3+} will act as a network former. This concept

is known as the charge-compensation effect, and has become generally accepted. Due to its ability to act both as a network former and a network modifier, $\text{AlO}_{1.5}$ and $\text{FeO}_{1.5}$ are termed "amphoteric" components.

The thermodynamic database of the MQM parameters, which the viscosity model is based on to determine $x_{\text{Si-Si}}$, does not consider the different structural roles of Al^{3+} and Fe^{3+} because the thermodynamic properties do not strongly depend on the different structural states. Therefore, to model a viscosity maximum induced by the amount of network-forming Al^{3+} and Fe^{3+} in a slag, they have to be separately evaluated.

It is assumed that the charge-compensated Al^{3+} and Fe^{3+} in the silicate network have the same impact on viscosity as Si^{4+} . The quantity of network-forming associate species, in relation to temperature and composition, can be determined from the equilibrium constant (K) of the following equilibria, Equations (7.11) to (7.14).



The concentrations of the associate species, $x_{\text{CaAl}_2}^{s_1}$, $x_{\text{MgAl}_2}^{s_1}$, $x_{\text{FeAl}_2}^{s_1}$ and $x_{\text{CaFe}_2}^{s_1}$ correspond to the concentration of network formers while the concentration of $x_{\text{Al}_{15}}^{s_1}$, $x_{\text{Fe}}^{s_1}$ and $x_{\text{Fe}_{15}}^{s_1}$ corresponds to the concentration of network modifiers. By increasing the Si content by the amount of the associate species calculated from Equations (7.11) to (7.14) it is possible to estimate values of A and E for Al-containing systems with Equation (7.6) and Equation (7.7).

Therefore, to accurately model the viscosity, equilibrium constants, Equations (7.16) to (7.19), of the reactions are required.

$$K_{\text{CaAl}_2} = \frac{a_{\text{CaAl}_2}}{a_{\text{Al}}^2 \cdot a_{\text{Ca}}} \quad (7.16)$$

$$K_{\text{MgAl}_2} = \frac{a_{\text{MgAl}_2}}{a_{\text{Al}}^2 \cdot a_{\text{Mg}}} \quad (7.17)$$

$$K_{\text{FeAl}_2} = \frac{a_{\text{FeAl}_2}}{a_{\text{Al}}^2 \cdot a_{\text{FeO}}} \quad (7.18)$$

$$K_{\text{CaFe}_2} = \frac{a_{\text{CaFe}_2}}{a_{\text{FeO}_{1.5}}^2 \cdot a_{\text{Ca}}} \quad (7.19)$$

$$(7.20)$$

The activity coefficients a_i of the species Al, Na, Ca, and Mg can be obtained from the implemented MQM model in FactSage. However, the activities of the associated species are not available, as they are not included in the thermodynamic database. Therefore, it is assumed that the activities of all species in Equations (7.16) to (7.19) can be approximated by their concentrations, i.e., $x_i^{s_1}$.

Using an equation for K , the concentration of an associate species can be determined by calculating the Gibbs free energy of the reaction, Equation (7.21), coupled with an optimised value for ΔG° , from Table 7.2.

$$\Delta G^\circ = -RT \ln K \quad (7.21)$$

An example case is provided for Equation (7.11) to determine the composition of the associate species $x_{\text{CaAl}_2}^{\mathcal{S}_1}$, using the combined equations Equations (7.16) and (7.21) and the optimised value of $\Delta G_{\text{CaAl}_2}^\circ$ from Table 7.2. The combined equation, Equation (7.22), is expressed in terms of compositions $x_i^{\mathcal{S}_1}$, with the superscript \mathcal{S}_1 indicating compositions that now include the associate species.

$$5000 - 100000x_{\text{Si}}^{\mathcal{S}_0} = -RT \ln \frac{(x_{\text{CaAl}_2}^{\mathcal{S}_1})}{(x_{\text{Al}}^{\mathcal{S}_1})^2 \cdot (x_{\text{Ca}}^{\mathcal{S}_1})} \quad (7.22)$$

The compositions $x_{\text{CaAl}_2}^{\mathcal{S}_1}$, $x_{\text{Ca}}^{\mathcal{S}_1}$, and $x_{\text{Al}}^{\mathcal{S}_1}$ can be expressed in terms of n_i with Equations (7.23) to (7.27).

$$x_{\text{CaAl}_2}^{\mathcal{S}_1} = \frac{n_{\text{CaAl}_2}^{\mathcal{S}_1}}{n_{\text{Total}}^{\mathcal{S}_1}} = \frac{n_{\text{CaAl}_2}^{\mathcal{S}_1}}{(n_{\text{CaAl}_2}^{\mathcal{S}_1} + n_{\text{Al}}^{\mathcal{S}_1} + n_{\text{Ca}}^{\mathcal{S}_1})} \quad (7.23)$$

$$x_{\text{Ca}}^{\mathcal{S}_1} = \frac{n_{\text{Ca}}^{\mathcal{S}_1}}{n_{\text{Total}}^{\mathcal{S}_1}} = \frac{n_{\text{Ca}}^{\mathcal{S}_1}}{(n_{\text{CaAl}_2}^{\mathcal{S}_1} + n_{\text{Al}}^{\mathcal{S}_1} + n_{\text{Ca}}^{\mathcal{S}_1})} \quad (7.24)$$

$$x_{\text{Al}}^{\mathcal{S}_1} = \frac{n_{\text{Al}}^{\mathcal{S}_1}}{n_{\text{Total}}^{\mathcal{S}_1}} = \frac{n_{\text{Al}}^{\mathcal{S}_1}}{(n_{\text{CaAl}_2}^{\mathcal{S}_1} + n_{\text{Al}}^{\mathcal{S}_1} + n_{\text{Ca}}^{\mathcal{S}_1})} \quad (7.25)$$

$$n_{\text{Ca}}^{\mathcal{S}_1} = n_{\text{Ca}}^{\mathcal{S}_0} - n_{\text{CaAl}_2}^{\mathcal{S}_1} \quad (7.26)$$

$$n_{\text{Al}}^{\mathcal{S}_1} = n_{\text{Al}}^{\mathcal{S}_0} - 2n_{\text{CaAl}_2}^{\mathcal{S}_1} \quad (7.27)$$

A careful evaluation of Equations (7.22) to (7.27) reveals that $n_{\text{CaAl}_2}^{\mathcal{S}_1}$ is the only unknown. This value can be determined through a root-finding procedure constrained by an elemental mass balance, ensuring the correct root is selected to satisfy mass conservation.

For $\text{MeO}_x - \text{AlO}_{1.5}/\text{FeO}_{1.5} - \text{SiO}_2$ systems, ΔG° varies linearly as a function of SiO_2 content, with no temperature dependence. It becomes more negative with increasing SiO_2 concentration (Kim 2011).

Finally, calculating A and E using Equation (7.6) and Equation (7.7) requires updating the mole fractions to “equivalent” mole fractions $x_i^{\mathcal{S}_2}$, as shown in Equations (7.28) to (7.31). This adjustment accounts for the network-forming effect of the associated species. In this approach, the slag is considered to have the same viscosity as an “equivalent” slag without network-forming Al^{3+} , which is compensated by $x_i^{\mathcal{S}_2}$.

$$x_{Si}^{s_2} = [x_{Si}^{s_1} + 2x_{CaAl_2}^{s_1} + 2x_{MgAl_2}^{s_1} + 2x_{FeAl_2}^{s_1} + 2x_{CaFe_2}^{s_1}]/N_{tot} \quad (7.28)$$

$$x_{Al}^{s_2} = [x_{Al}^{s_1}]/N_{tot} \quad (7.29)$$

$$x_{Ca}^{s_2} = [x_{Ca}^{s_1}]/N_{tot} \quad (7.30)$$

$$x_{Mg}^{s_2} = [x_{Mg}^{s_1}]/N_{tot} \quad (7.31)$$

$$x_{FeO}^{s_2} = [x_{FeO}^{s_1}]/N_{tot} \quad (7.32)$$

$$x_{FeO_{1.5}}^{s_2} = [x_{FeO_{1.5}}^{s_1}]/N_{tot} \quad (7.33)$$

$$(7.34)$$

with:

$$N_{tot} = x_{Si}^{s_1} + x_{Al}^{s_1} + x_{Ca}^{s_1} + x_{Mg}^{s_1} + x_{FeO}^{s_1} + x_{FeO_{1.5}}^{s_1} + 2x_{CaAl_2}^{s_1} + 2x_{MgAl_2}^{s_1} + 2x_{FeAl_2}^{s_1} + 2x_{CaFe_2}^{s_1} \quad (7.35)$$

7.1.5 Variable Declarations

Table 7.1: Optimised viscosity parameters

System	A (Pa s)	E (J mol ⁻¹)
SiO ₂	$A_{Si}^* = -10.56$	$E_{SiO_2}^* = 217200$
	$A_{Si}^E = -6.13$	$E_{SiO_2}^E = 298500$
AlO _{1.5}	$A_{Al_{1.5}} = -9.22$	$E_{Al} = 120400$
CaO	$A_{Ca} = -12.27$	$E_{Ca} = 137650$
MgO	$A_{Mg} = -10.58$	$E_{Mg} = 117160$
FeO	$A_{Fe} = -8.75$	$E_{Fe} = 52500$
FeO _{1.5}	$A_{Fe_{1.5}} = -8.63$	$E_{Fe_{1.5}} = 47250$
SiO ₂ – AlO _{1.5}	$A_{Al-Si}^R = -12.30$	$E_{Al-Si} = -75000$
		$E_{Al-Si}^R = 303500$
SiO ₂ – CaO	-	$E_{Ca-Si} = -101750$
		$E_{Ca-Si}^R = 81400$
SiO ₂ – MgO	-	$E_{Mg-Si} = -86250$
		$E_{Mg-Si}^R = 72600$
SiO ₂ – FeO	-	$E_{Fe-Si} = -115000$
		$E_{Fe-Si}^R = 87525$
SiO ₂ – FeO _{1.5}	-	$E_{Fe_{1.5}-Si} = -107500$
		$E_{Fe_{1.5}-Si}^R = 88500$

Table 7.2: Optimised values of ΔG° for the associate species for slag systems containing AlO_{1.5} (Grundy et al. 2008a).

System	
CaO – AlO _{1.5} – SiO ₂	$\Delta G_{CaAl_2}^\circ = 5000 - 100000x_{Si}^{s_0}$
MgO – AlO _{1.5} – SiO ₂	$\Delta G_{MgAl_2}^\circ = 13000 - 105000x_{Si}^{s_0}$
FeO – AlO _{1.5} – SiO ₂	$\Delta G_{FeAl_2}^\circ = -66944x_{Si}^{s_0}$
CaO – FeO _{1.5} – SiO ₂	$\Delta G_{CaFe_2}^\circ = 2092 - 5335x_{Si}^{s_0}$

7.1.6 Assumptions

The following assumptions was made to formulate this model.

1. Where no experimental data were available, viscosity parameters for unary systems are extrapolated from binary viscosity data.
2. For pure silica, two contributions to the viscosity are assumed. The first is that there is a contribution to viscosity that is independent on the formation of a polymer network. The second is that the silicate network itself contributes to the viscosity.
3. It is assumed that the effect of network-forming Al^{3+} and Fe^{3+} on the viscosity will be the same as that of Si^{4+} .
4. For solving the equilibrium equations of the associate species, the activities of all species are assumed to be accurately approximated by their concentrations.
5. For systems not containing Al_2O_3 or Fe_2O_3 it is assumed that $\ln(\mu)$ can be calculated from a linear combination of A and E of binary systems.

7.1.7 Simplifications

The following simplifications was made in this model. The critical group size for SiO_4 clusters is set to be $n = 40$ interconnected Si – Si pairs. Also, the interaction between MgO and Fe_2O_3 is not accounted for as it is for that between CaO and Fe_2O_3 .

7.1.8 Literature Inaccuracies

Background

During development of the multicomponent model catered for systems containing Al_2O_3 , we experienced significant difficulty to navigate uncertainties caused by literature inaccuracies. To ensure the user do not go through the same trouble, these are listed here.

Inaccuracies

1. Calculating ΔG

Grundy et al. (2008a) reported that ΔG which dictates the equilibrium constant for the formation of CaAl_2O_4 and MgAl_2O_4 should be calculated as

$$\Delta G_{\text{CaAl}_2}^{\circ} = 5000 - 100000x_{\text{Si}}^{s_0} \text{ and } \Delta G_{\text{MgAl}_2}^{\circ} = 13000 - 105000x_{\text{Si}}^{s_0},$$

while Kim et al. (2012a) reported

$$\Delta G_{\text{CaAl}_2}^{\circ} = -5000 - 100000x_{\text{Si}}^{s_0} \text{ and } \Delta G_{\text{MgAl}_2}^{\circ} = -13000 - 105000x_{\text{Si}}^{s_0}.$$

Grundy et al. (2008a) reported it correctly.

2. Calculating x^{s_2}

Grundy et al. (2008a) reported the calculation of $x_{\text{Si}}^{s_2}$ to be

$$x_{\text{Si}}^{s_2} = [x_{\text{Si}}^{s_1} + x_{\text{NaAl}}^{s_1} + 2x_{\text{CaAl}_2}^{s_1} + 2x_{\text{MgAl}_2}^{s_1}]/N_{\text{tot}} \quad (7.36)$$

where

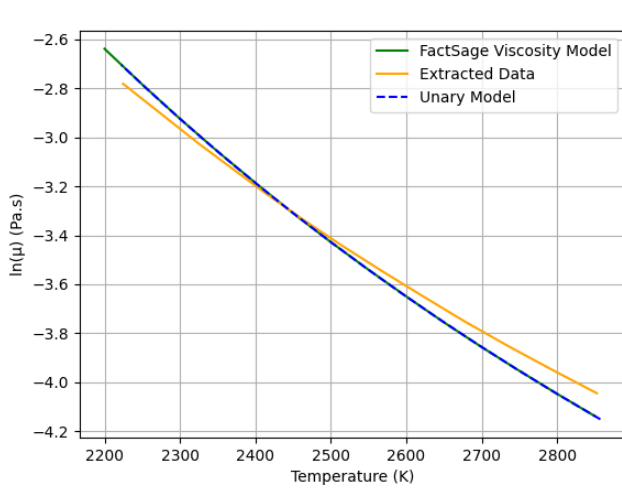
$$N_{\text{tot}} = x_{\text{Si}}^{\text{S}_1} + x_{\text{Al}}^{\text{S}_1} + x_{\text{Na}}^{\text{S}_1} + x_{\text{Ca}}^{\text{S}_1} + x_{\text{Mg}}^{\text{S}_1} - x_{\text{NaAl}}^{\text{S}_1} - x_{\text{CaAl}_2}^{\text{S}_1} - x_{\text{MgAl}_2}^{\text{S}_1} \quad (7.37)$$

while Kim et al. (2012a) reported the same calculation for $x_{\text{Si}}^{\text{S}_2}$ but with

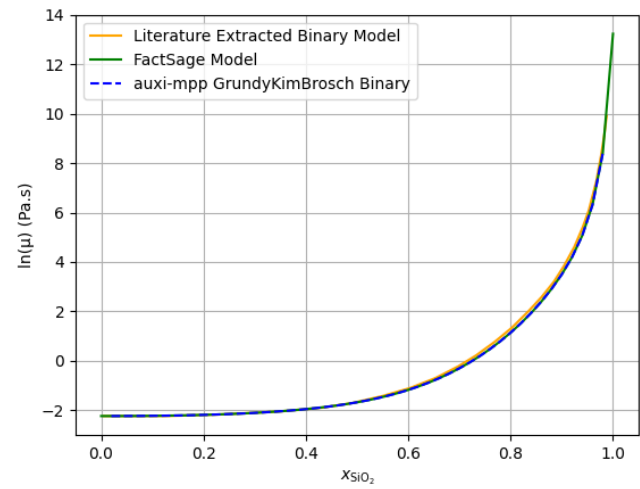
$$N_{\text{tot}} = x_{\text{Si}}^{\text{S}_1} + x_{\text{Al}}^{\text{S}_1} + x_{\text{Na}}^{\text{S}_1} + x_{\text{Ca}}^{\text{S}_1} + x_{\text{Mg}}^{\text{S}_1} + x_{\text{NaAl}}^{\text{S}_1} + 2x_{\text{CaAl}_2}^{\text{S}_1} + 2x_{\text{MgAl}_2}^{\text{S}_1} \quad (7.38)$$

Here, Kim et al. (2012a) reported it correctly.

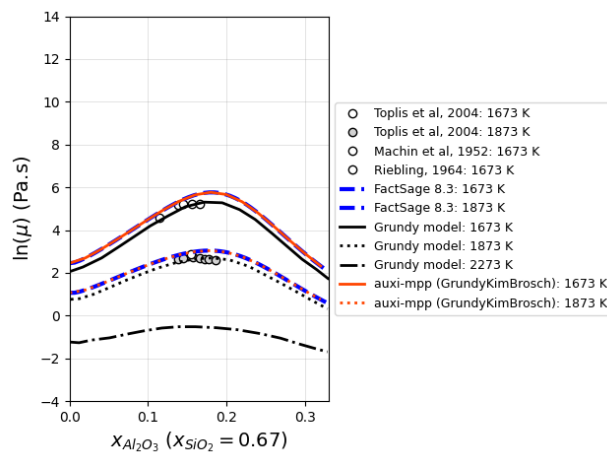
3. Incorrect plots presented in Grundy et al. (2008b) and Grundy et al. (2008a).



(a) Al_2O_3 – Grundy et al. (2008b) Fig. 7. 'Ex-tracted Data' represents Grundy's model and 'Unary Model' represents auxi-mpp's model.



(b) Al_2O_3 – SiO_2 – Grundy et al. (2008b) Fig. 8. 'Literature Extracted Binary Model' represents Grundy's model.



(c) Al_2O_3 – MgO – SiO_2 – Grundy et al. (2008a) Fig. 32

Figure 7.1: Inaccurate plots.

The seemingly small deviation present in Figure 7.1b at $x_{\text{SiO}_2} = 0.8$, was found to be double the deviation found in Figure 7.1a at $T = 2800\text{K}$. These deviations were confirmed not to be due to erroneous data extraction. The deviation in Figure 7.1c is

also a definite inaccuracy since Fig. 31 and 33 matches correctly with auxi-mpp and FactSage's model, and Grundy's binary model agrees with the calculated viscosity at $x_{\text{Al}_2\text{O}_3} = 0$. The same problem is present for Fig. 23 of Grundy et al. (2008a).

4. Incorrect plot presented in Kim et al. (2021a).

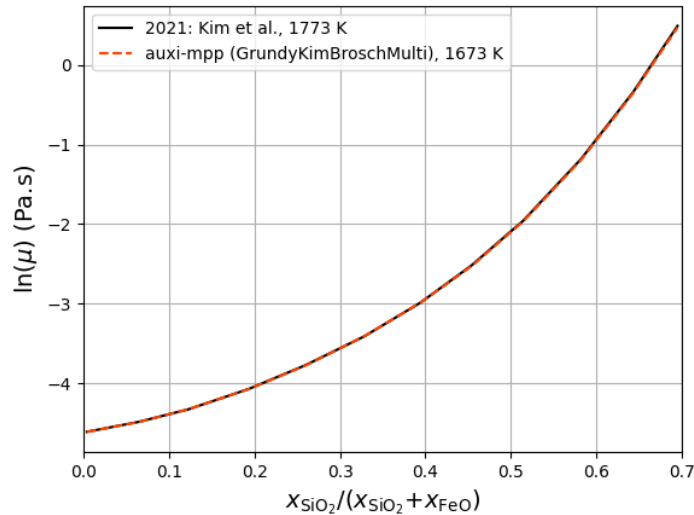


Figure 7.2: CaO – FeO – SiO₂

In Figure 7.2, auxi-mpp plotted the same compositions but 100 K lower than the literature plot at 1773 K. There is an exact match, implying that Kim et al. (2021a) provided the incorrect temperature label.

5. Incorrect plot section defined.

The original figure from which the literature data in Figure 7.2 were extracted is Figure 9 in Kim et al. (2021a). The section to plot is there defined as (81.24 mol % FeO, 13.76 mol % CaO) to (86.75 mol % SiO₂, 13.25 mol % CaO). The first endpoint does not border and is therefore incorrect. The correct endpoint is **(86.24 mol % FeO, 13.76 mol % CaO)**.

7.1.9 Model Validation

This section details the current status of the Grundy-Kim-Brosch viscosity model implementation in auxi-mpp and presents results for various slag systems. The auxi-mpp model results were compared against the literature model and experimental data extracted from Grundy et al. (2008b), Grundy et al. (2008a), Kim et al. (2021a), and Kim et al. (2021b). auxi-mpp were validated by means of literature figure reproduction as well as with a correlation plot. Validation by figure reproduction is summarised in Table 7.3, and those by correlation plot is listed thereafter.

Table 7.3: Viscosity Validation Ranges

Model	Systems	Composition (mol mol ⁻¹)	Temperature (K)
Unary	SiO ₂	pure substance	1250 – 3250
	FeO	pure substance	1100 – 2100
	Fe ₂ O ₃	pure substance	1100 – 1850
Binary	Al ₂ O ₃ – SiO ₂	$x_{\text{Al}_2\text{O}_3} = 0 - 1$	2073, 2173
	CaO – SiO ₂	$x_{\text{CaO}} = 0 - 1$	1773, 1873, 2073
	MgO – SiO ₂	$x_{\text{MgO}} = 0 - 1$	1773, 1873, 2073
	FeO – SiO ₂	$x_{\text{FeO}} = 0.3 - 1$	1473, 1573, 1673, 1773
Ternary	CaO – MgO – SiO ₂	$y_{\text{SiO}_2} = 0.3 - 0.75, y_{\text{SiO}_2}/y_{\text{MgO}} = 1$	1673, 1773, 1873
	CaO – MgO – SiO ₂	$y_{\text{SiO}_2} = 0.3 - 0.8, y_{\text{MgO}} = 0.2$	1673, 1773, 1873
	Al ₂ O ₃ – CaO – SiO ₂	$x_{\text{Al}_2\text{O}_3} = 0.0 - 0.33, x_{\text{SiO}_2} = 0.67$	1673, 1873
	Al ₂ O ₃ – CaO – SiO ₂	$x_{\text{Al}_2\text{O}_3} = 0.0 - 0.25, x_{\text{SiO}_2} = 0.75$	1673, 1873
	Al ₂ O ₃ – MgO – SiO ₂	$x_{\text{Al}_2\text{O}_3} = 0.0 - 0.50, x_{\text{SiO}_2} = 0.50$	1673, 1873
	Al ₂ O ₃ – MgO – SiO ₂	$x_{\text{Al}_2\text{O}_3} = 0.0 - 0.33, x_{\text{SiO}_2} = 0.67$	1673, 1873
	Al ₂ O ₃ – MgO – SiO ₂	$x_{\text{Al}_2\text{O}_3} = 0.0 - 0.25, x_{\text{SiO}_2} = 0.75$	1673, 1873
Quaternary	Al ₂ O ₃ – CaO – MgO – SiO ₂	$y_{\text{Al}_2\text{O}_3} = 0.0 - 0.45, y_{\text{SiO}_2} = 0.5, y_{\text{MgO}} = 0.05$	1773
	Al ₂ O ₃ – CaO – MgO – SiO ₂	$y_{\text{Al}_2\text{O}_3} = 0.0 - 0.35, y_{\text{SiO}_2} = 0.5, y_{\text{MgO}} = 0.15$	1773
	Al ₂ O ₃ – CaO – MgO – SiO ₂	$y_{\text{Al}_2\text{O}_3} = 0.0 - 0.25, y_{\text{SiO}_2} = 0.5, y_{\text{MgO}} = 0.25$	1773

Fe-bearing systems validated by means of correlation plots;

1. Al₂O₃ – FeO – SiO₂
2. Fe₂O₃ – FeO – SiO₂
3. Al₂O₃ – CaO – FeO – SiO₂
4. FeO – MgO – SiO₂
5. CaO – Fe₂O₃ – FeO – SiO₂
6. CaO – FeO – MgO – SiO₂
7. Al₂O₃ – CaO – FeO – MgO – SiO₂
8. Al₂O₃ – FeO – MgO – SiO₂

See Figure 7.8.

Unary Systems

Figure 7.3 demonstrates the agreement between [auxi-mpp](#) and the literature model for unary systems, plotting the natural logarithm of viscosity against temperature.

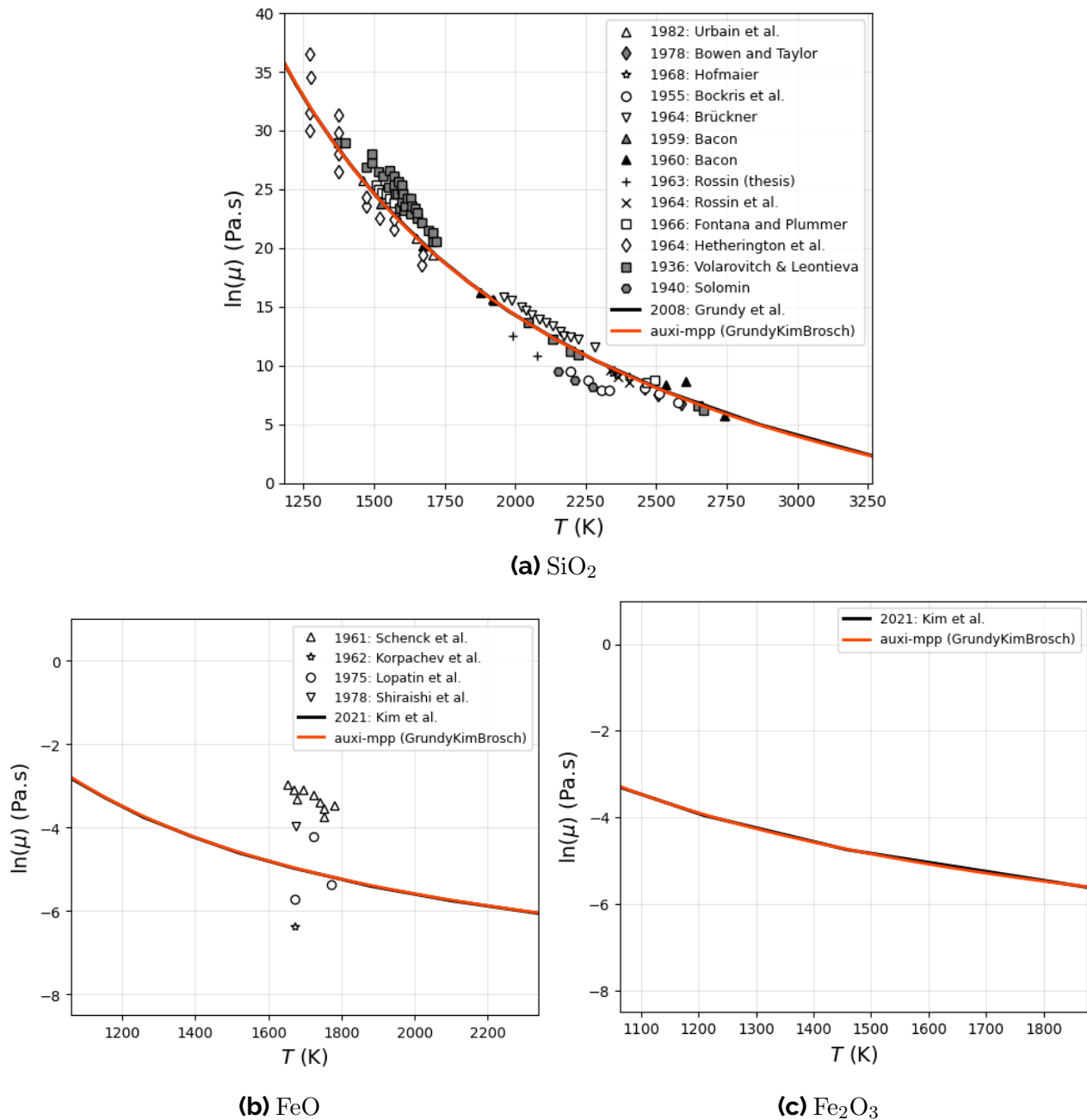


Figure 7.3: Viscosity model estimates and comparison for pure SiO_2 , FeO and Fe_2O_3 .

Binary Systems

Figure 7.4 illustrates the accuracy of the Grundy-Kim-Brosch model ("auxi-mpp GrundyKimBrosch") for estimating viscosities in binary $\text{Al}_2\text{O}_3 - \text{SiO}_2$, $\text{CaO} - \text{SiO}_2$, and $\text{MgO} - \text{SiO}_2$ systems. Note that validations above 2200 K were intentionally omitted.

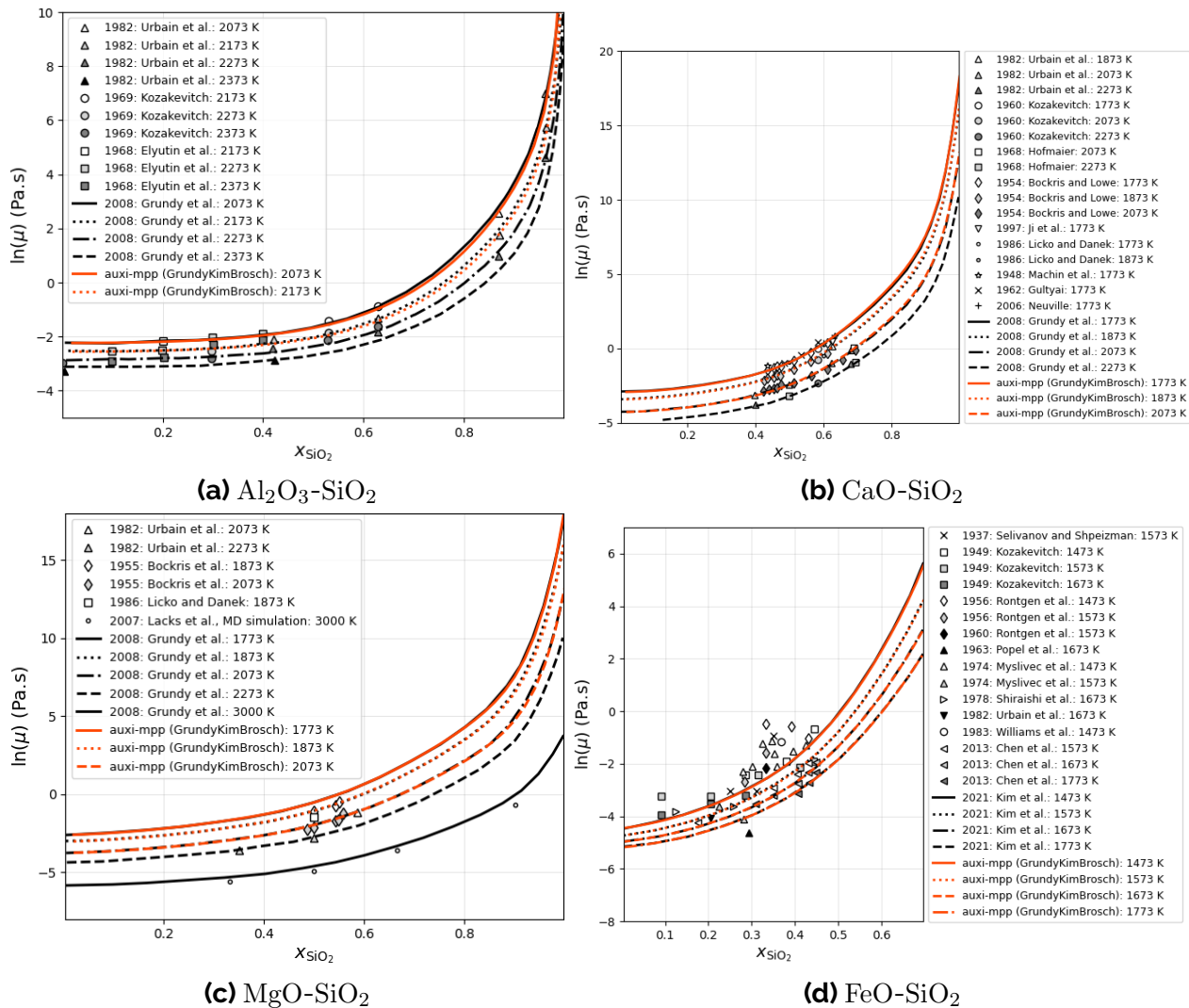


Figure 7.4: Viscosity model estimates and comparisons for binary slag systems.

Multicomponent Systems

Ternary systems without Al_2O_3 were validated initially, as the Grundy-Kim-Brosch model does not require consideration of the charge compensation effect of Al_2O_3 on slag viscosity (Kim 2011; Grundy et al. 2008a). Figure 7.5 demonstrates that viscosity estimates for systems of SiO_2 – MgO – CaO closely align with both model estimates and experimental data from the literature (Grundy et al. 2008a).

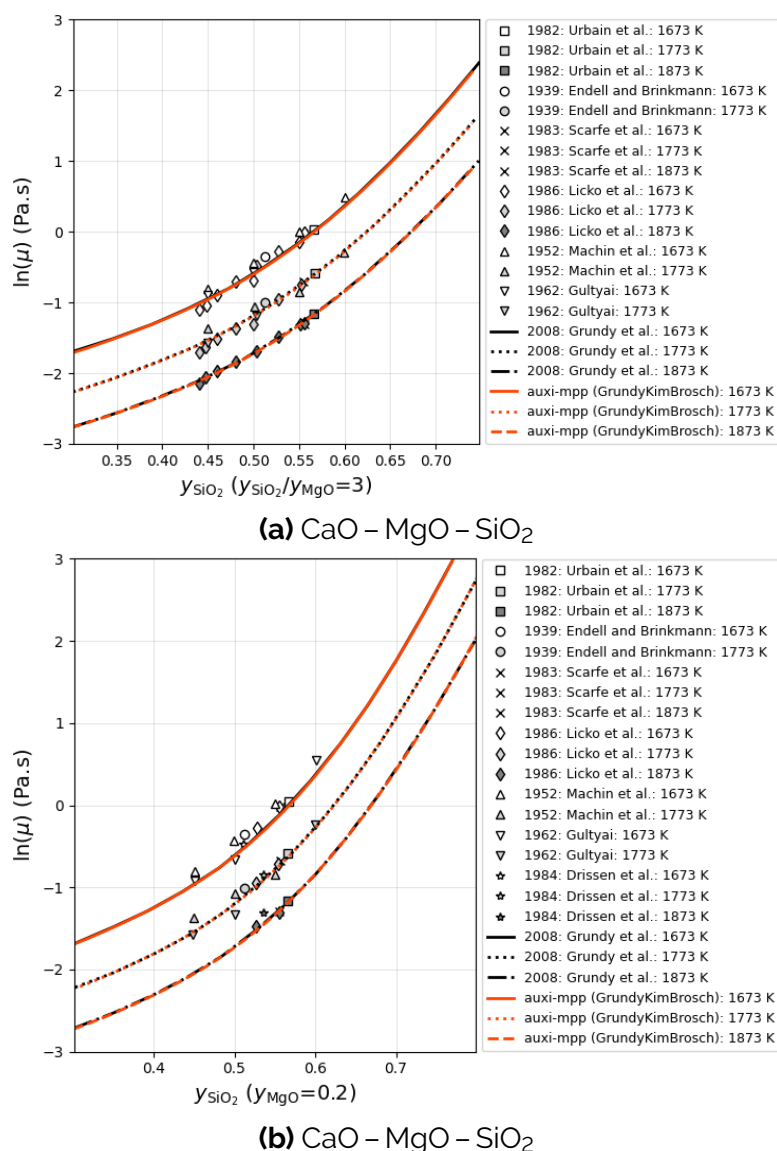


Figure 7.5: Viscosity model estimates for ternary slag systems without alumina.

Some peculiar results were obtained when validating the model for systems containing Al₂O₃ as seen in Figure 7.6. In Figure 7.6a and Figure 7.6d we reason that the literature plots are incorrect. To support this, the results of FactSage 8.3 were added for comparison. In Figure 7.6d the auxi-mpp model follows the result of FactSage, confirming that the auxi-mpp implementation is correct. This was also applied to Figure 7.6a, however it seems like FactSage's model does not correctly estimate viscosity for systems containing CaO. At the extremes, the auxi-mpp model agrees with FactSage's model, however.

Another reason why these two literature figures are incorrect is that the auxi-mpp binary model, that were successfully validated for the relevant systems, agrees with the multi-component auxi-mpp model at $x_{\text{Al}_2\text{O}_3} = 0.0$.

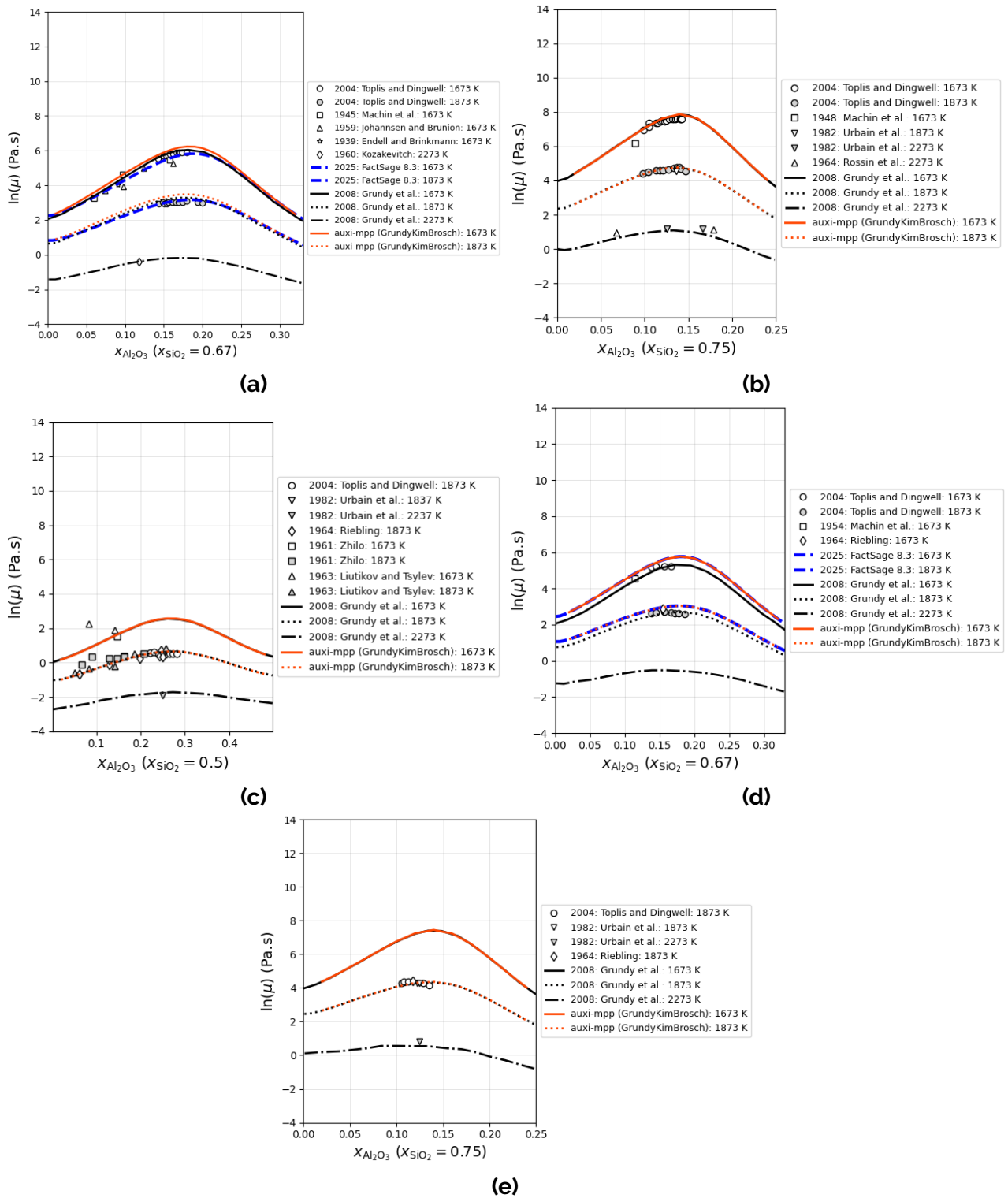


Figure 7.6: Viscosity model estimates for ternary slag systems containing alumina.

The multicomponent viscosity model was successfully validated for the $Al_2O_3 - CaO - MgO - SiO_2$ system for a range of compositions at 1773 K as shown in Figure 7.7.

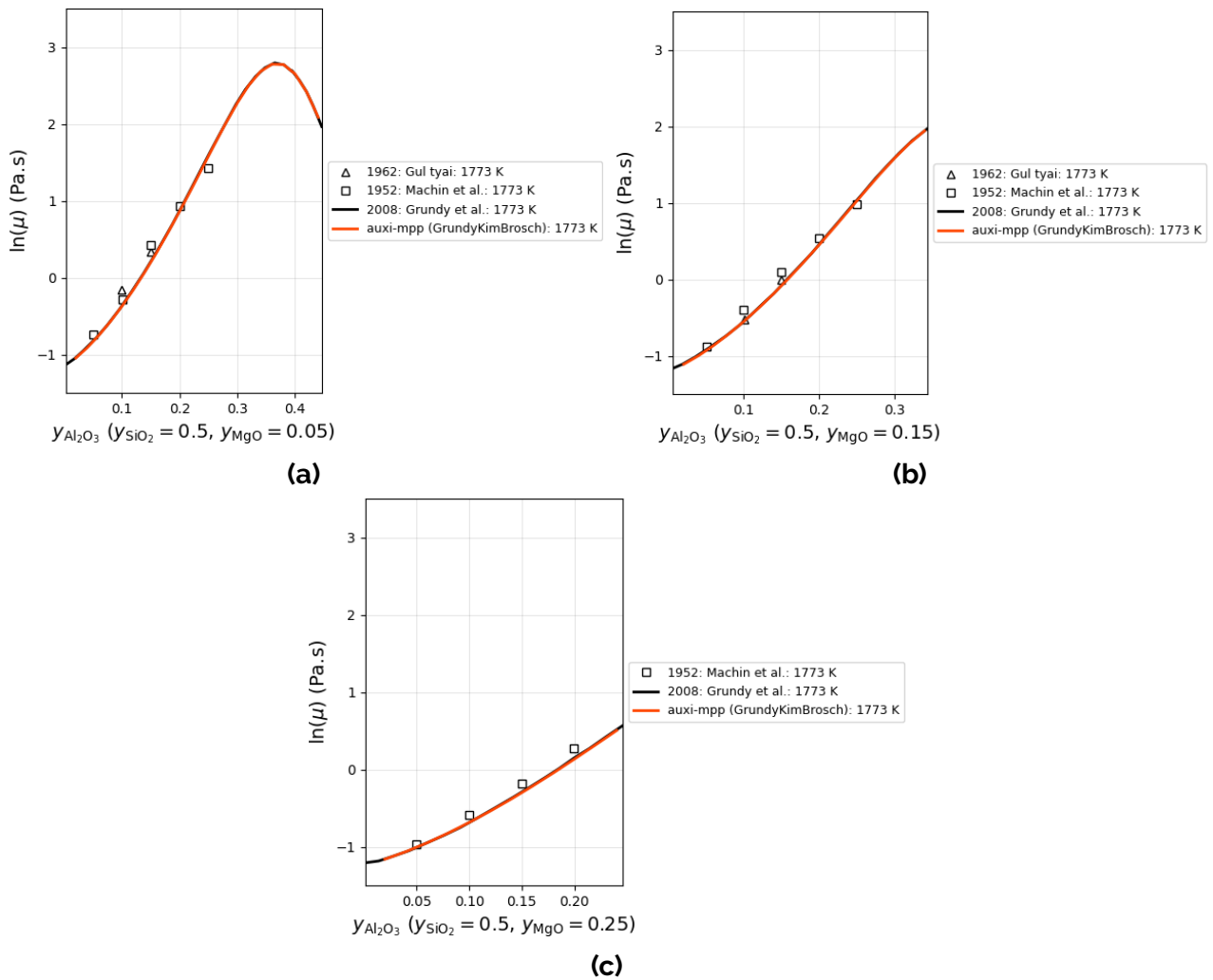


Figure 7.7: Viscosity model estimates for the $\text{Al}_2\text{O}_3 - \text{CaO} - \text{MgO} - \text{SiO}_2$ quaternary slag system at 1773 K.

Multicomponent Fe-bearing Systems

The available data for multi-component Fe-bearing systems often have abstract axes making it time-consuming to reproduce. These systems are therefore validated by means of correlation plots. Figure 7.8 shows how [auxi-mpp](#) performs, with systems containing either FeO or Fe_2O_3 or both, compared to Kim's model as presented in literature (Kim et al. 2021a; Kim et al. 2021b).

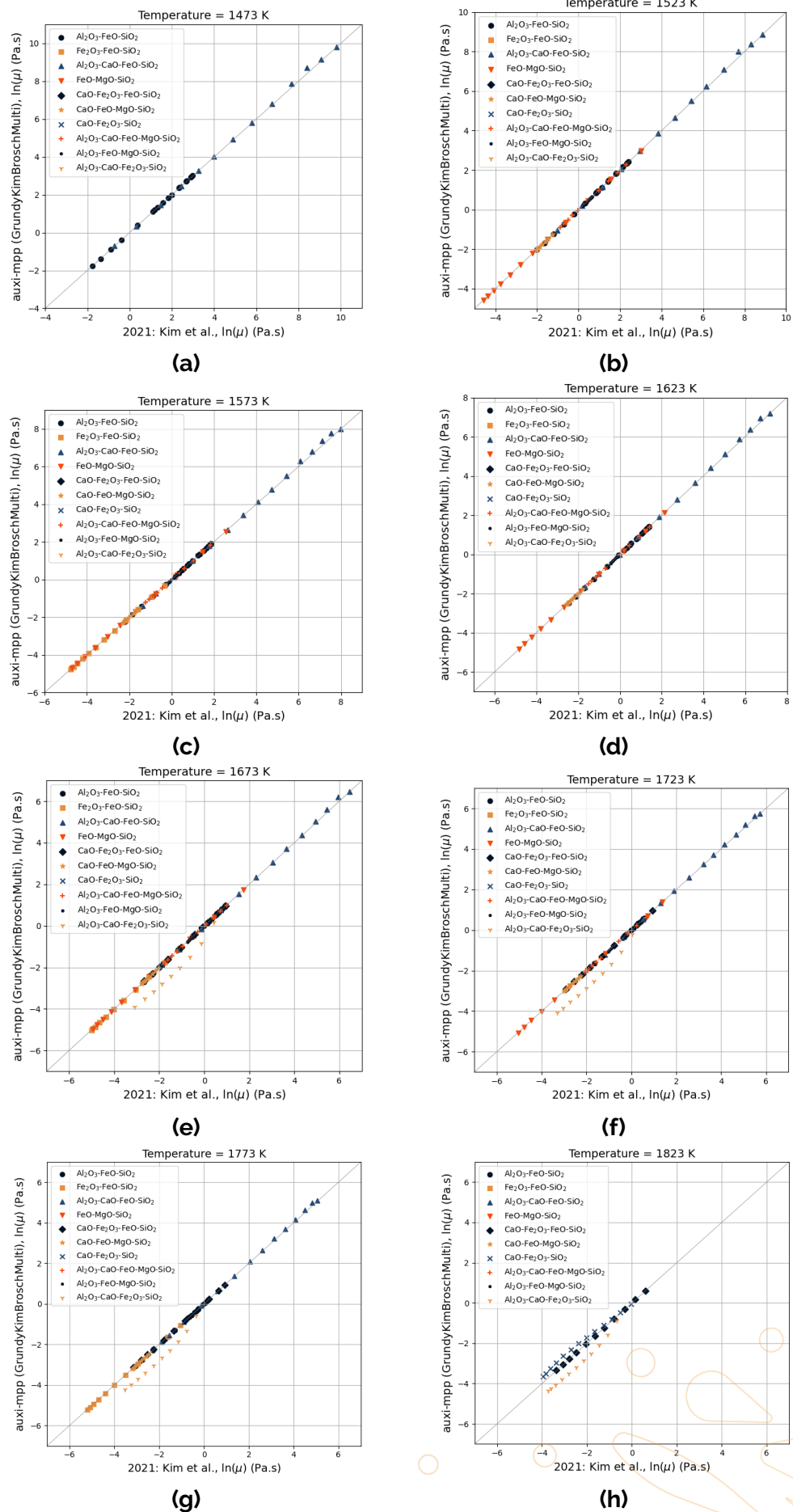


Figure 7.8: auxi-mpp vs Kim et al. (2021b) correlation plots.

For most systems [auxi-mpp](#) performs well. There are two systems for which there are visible deviation from literature, however. These are $\text{CaO} - \text{Fe}_2\text{O}_3 - \text{SiO}_2$ and $\text{Al}_2\text{O}_3 - \text{CaO} - \text{Fe}_2\text{O}_3 - \text{SiO}_2$. For $\text{CaO} - \text{Fe}_2\text{O}_3 - \text{SiO}_2$ the original figure were reproduced in Figure 7.9, adding the performance of [FactSage 8.3's](#) (2025) viscosity model. [auxi-mpp](#) plots close to but not exactly on top of [FactSage](#), and both deviates significantly from literature. Whether this is an error in literature or if both [auxi-mpp](#) and [FactSage](#) are incorrect, is uncertain. It is also possible that this is caused by a parameter change in [FactSage's](#) FToxid database in the time period of 2021 to 2025.

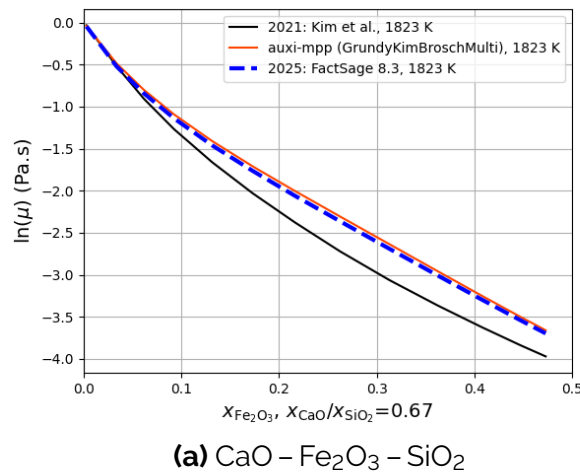


Figure 7.9: [auxi-mpp](#) vs [FactSage 8.3](#) (2025) vs Kim et al. (2021b).

The issue with $\text{Al}_2\text{O}_3 - \text{CaO} - \text{Fe}_2\text{O}_3 - \text{SiO}_2$ is similar as [auxi-mpp's](#) results is close to [FactSage 8.3](#), with both deviating significantly from literature.

Issues

Potential issue with the systems $\text{CaO} - \text{Fe}_2\text{O}_3 - \text{SiO}_2$ and $\text{Al}_2\text{O}_3 - \text{CaO} - \text{Fe}_2\text{O}_3 - \text{SiO}_2$. See Figures 7.8 and 7.9.

Part III

Appendices



Appendix A

Definitions

The following definitions apply to manual.

EM-MPPF means the Ex Mente Material Physical Property Framework.

EM-MPP-STK means the Ex Mente Material Physical Property Simulation Toolkit, which is a Python package.

EM-AMDF refers to the Ex Mente Accelerated Material Description Framework.

The Slag Sub-package means a sub-package of [EM-MPP-STK](#) that contains slag physical property models and their parameters and the necessary documentation.

REF processes means Reducing Electric Furnace processes.

REF-MPP means Reducing Electric Furnace Material Physical Property.

MQM means Modified Quasichemical Model

ChemApp for Python means the ChemApp for Python package for computational thermochemistry owned by GTT-Technologies.

FactSage means the FactSage suite for computational thermochemistry owned by GTT-Technologies.

auxi-mpp is the python package containing all material physical property models, where 'auxi' means help, and 'mpp' means material physical properties.

References

- Brosh, E., A. Pelton, and S. Decterov (May 2012). "A Model to Calculate the Viscosity of Silicate Melts. Part IV: Borosilicate Melts Containing Alkali Metals". In: *International Journal of Materials Research (formerly Zeitschrift fuer Metallkunde)* 103, p. 537. DOI: [10.3139/146.110639](https://doi.org/10.3139/146.110639).
- Grundy, A. N., I.-H. Jung, A. D. Pelton, and S. A. Decterov (2008a). "A Model to Calculate the Viscosity of Silicate Melts. Part II: The NaO0.5–MgO–CaO–AlO1.5–SiO2 System". In: *International Journal of Materials Research* 99.11, pp. 1195–1209. DOI: [doi:10.3139/146.101753](https://doi.org/10.3139/146.101753). (Visited on 08/22/2023).
- Grundy, A. N., H. Liu, I.-H. Jung, S. A. Decterov, and A. D. Pelton (2008b). "A Model to Calculate the Viscosity of Silicate Melts. Part I: Viscosity of Binary SiO2–MeOx Systems (Me = Na, K, Ca, Mg, Al)". In: *International Journal of Materials Research* 99.11, pp. 1185–1194. DOI: [doi:10.3139/146.101752](https://doi.org/10.3139/146.101752). (Visited on 08/22/2023).
- Hundermark, R. (2003). "The Electrical Conductivity of Melter Type Slags". Master of Engineering, MEng. Cape Town, South Africa: University of Cape Town.
- Kim, W. Y. (Aug. 2011). "Modeling Viscosity of Molten Slags and Glasses". PhD thesis. École Polytechnique de Montréal. (Visited on 09/11/2024).
- Kim, W.-Y., P. Hudon, and I.-H. Jung (Mar. 1, 2021a). "Modeling the viscosity of silicate melts containing Fe oxide: Fe saturation condition". In: *Calphad* 72, p. 102242. ISSN: 0364-5916. DOI: [10.1016/j.calphad.2020.102242](https://doi.org/10.1016/j.calphad.2020.102242). URL: <https://www.sciencedirect.com/science/article/pii/S0364591620305058> (visited on 10/18/2024).
- Kim, W.-Y., P. Hudon, and I.-H. Jung (Mar. 1, 2021b). "Modeling the viscosity of silicate melts containing Fe oxide: FeO/Fe2O3 containing system". In: *Calphad* 72, p. 102244. ISSN: 0364-5916. DOI: [10.1016/j.calphad.2020.102244](https://doi.org/10.1016/j.calphad.2020.102244). URL: <https://www.sciencedirect.com/science/article/pii/S0364591620305071> (visited on 08/22/2023).
- Kim, W.-Y., A. D. Pelton, and S. A. Decterov (2012a). "A Model to Calculate the Viscosity of Silicate Melts. Part III: Modification for Melts Containing Alkali Oxides". In: *International Journal of Materials Research* 103.3, pp. 313–328. DOI: [doi:10.3139/146.110637](https://doi.org/10.3139/146.110637). (Visited on 08/22/2023).
- Kim, W.-Y., A. D. Pelton, and S. A. Decterov (2012b). "A Model to Calculate the Viscosity of Silicate Melts. Part III: Modification for Melts Containing Alkali Oxides". In: *Intern-*

tional Journal of Materials Research 103.3, pp. 313–328. DOI: [doi:10.3139/146.110637](https://doi.org/10.3139/146.110637). (Visited on 08/22/2023).

Mysen, B. and P. Richet (2019). *Silicate Glasses and Melts - 2nd Edition*. 2nd. Elsevier. ISBN: 978-0-444-63709-3. URL: <https://shop.elsevier.com/books/silicate-glasses-and-melts/mysen/978-0-444-63708-6> (visited on 10/03/2023).

Thibodeau, E. (2014). "Modeling the molar volume and electrical conductivity of oxide melts". MA thesis. Montreal, Canada: McGill University. (Visited on 06/26/2023).

Thibodeau, E. (Feb. 2016). "A structural electrical conductivity model for oxide melts". en. In: *METALLURGICAL AND MATERIALS TRANSACTIONS B* 47, pp. 355–383.

Thibodeau, E., A. E. Gheribi, and I.-H. Jung (2016a). "A Structural Molar Volume Model for Oxide Melts Part I: Li₂O-Na₂O-K₂O-MgO-CaO-MnO-PbO-Al₂O₃-SiO₂ Melts—Binary Systems". In: *Metallurgical and Materials Transactions B* 47.2, pp. 1147–1164. DOI: [doi:10.1007/s11663-015-0548-y](https://doi.org/10.1007/s11663-015-0548-y). (Visited on 06/13/2023).

Thibodeau, E., A. E. Gheribi, and I.-H. Jung (2016b). "A Structural Molar Volume Model for Oxide Melts Part II: Li₂O-Na₂O-K₂O-MgO-CaO-MnO-PbO-Al₂O₃-SiO₂ Melts—Ternary and Multicomponent Systems". In: *Metallurgical and Materials Transactions B* 47.2, pp. 1165–1186. DOI: [doi:10.1007/s11663-015-0543-3](https://doi.org/10.1007/s11663-015-0543-3). (Visited on 06/13/2023).

Thibodeau, E., A. E. Gheribi, and I.-H. Jung (2016c). "A Structural Molar Volume Model for Oxide Melts Part III: Fe Oxide-Containing Melts". In: *Metallurgical and Materials Transactions B* 47.2, pp. 1187–1202. DOI: [doi:10.1007/s11663-015-0549-x](https://doi.org/10.1007/s11663-015-0549-x). (Visited on 06/13/2023).

Glossaries

Acronyms

BF-BOF Blast Furnace-Basic Oxygen Furnace [2](#)

GGS Groeien met Groen Staal [i](#), [2](#)

MQM Modified Quasichemical Model [4](#), [9](#), [11–13](#), [20](#), [37](#), [38](#), [40](#), [41](#), [44](#)

REF Reducing Electric Furnace [i](#), [2](#)



Advancing Through Insight

